TISSUE ENGINEERING: Part A
Volume 19, Numbers 17 and 18, 2013

DOI: 10.1089/ten.tea.2012.0250

Production and Assessment of Decellularized Pig and Human Lung Scaffolds

Joan E. Nichols, PhD,[1] Jean Niles, MA,[1] Michael Riddle, MD,[1] Gracie Vargas, PhD,[2] Tuya Schilagard, PhD,[2] Liang Ma, PhD,[2] Kert Edward, PhD,[2] Saverio La Francesca,[3] Jason Sakamoto, PhD,[4] Stephanie Vega, BS,[2] Marie Ogadegbe, BS,[2] Ronald Mlcak, PhD,[5] Donald Deyo, DVM,[6] Lee Woodson, MD,[6] Christopher McQuitty, MD,[6] Scott Lick, MD,[7] Daniel Beckles, MD,[7] Esther Melo, MA,[8] and Joaquin Cortiella MD, MPH[6]

The authors have previously shown that acellular (AC) trachea-lung scaffolds can (1) be produced from natural rat lungs, (2) retain critical components of the extracellular matrix (ECM) such as collagen-1 and elastin, and (3) be used to produce lung tissue after recellularization with murine embryonic stem cells. The aim of this study was to produce large (porcine or human) AC lung scaffolds to determine the feasibility of producing scaffolds with potential clinical applicability. We report here the first attempt to produce AC pig or human trachea-lung scaffold. Using a combination of freezing and sodium dodecyl sulfate washes, pig trachea-lungs and human trachea-lungs were decellularized. Once decellularization was complete we evaluated the structural integrity of the AC lung scaffolds using bronchoscopy, multiphoton microscopy (MPM), assessment of the ECM utilizing immunocytochemistry and evaluation of mechanics through the use of pulmonary function tests (PFTs). Immunocytochemistry indicated that there was loss of collagen type IV and laminin in the AC lung scaffold, but retention of collagen-1, elastin, and fibronectin in some regions. MPM scoring was also used to examine the AC lung scaffold ECM structure and to evaluate the amount of collagen I in normal and AC lung. MPM was used to examine the physical arrangement of collagen-1 and elastin in the pleura, distal lung, lung borders, and trachea or bronchi. MPM and bronchoscopy of trachea and lung tissues showed that no cells or cell debris remained in the AC scaffolds. PFT measurements of the trachea-lungs showed no relevant differences in peak pressure, dynamic or static compliance, and a nonrestricted flow pattern in AC compared to normal lungs. Although there were changes in content of collagen I and elastin this did not affect the mechanics of lung function as evidenced by normal PFT values. When repopulated with a variety of stem or adult cells including human adult primary alveolar epithelial type II cells both pig and human AC scaffolds supported cell attachment and cell viability. Examination of scaffolds produced using a variety of detergents indicated that detergent choice influenced human immune response in terms of T cell activation and chemokine production.

Introduction

For patients with end-stage lung disease the only therapeutic option is often lung transplantation. Unfortunately, a number of these patients die from their disease because of the significant shortages of donated lungs for use in transplantation.[1,2] The current shortage in suitable donor lungs is also heightened by the fact that, due to its delicate nature, the lung is likely to be damaged or compromised during the process of organ donation and retrieval. This has led to the development of lung perfusion techniques and strategies used to recondition donor lungs, which initially do not meet standards for transplantation and may eventually increase the pool of acceptable organs.[3–7] For lungs that cannot be reconditioned there is still a way of potentially making them available for transplantation. By taking advantage of our ability to produce acellular (AC) natural lung scaffolds from discarded human lungs we could potentially use them to generate functional lung tissues. Although not a viable treatment option today, in the future lung tissue engineering may present a solution to the ever-increasing organ shortage problem.

Departments of [1]Internal Medicine, and [2]Bioengineering, University of Texas Medical Branch, Galveston, Texas.
[3]Department of Cardiovascular Surgery, Methodist Hospital, Houston, Texas.
[4]Methodist Research Institute, Houston, Texas.
[5]Department of Surgery, Shriners Hospital for Children, Galveston, Texas.
Departments of [6]Anesthesiology and [7]Surgery, University of Texas Medical Branch, Galveston, Texas.
[8]Unit of Physiological Sciences, University of Barcelona, Barcelona, Spain.

As we get closer to developing regenerative medicine strategies for tissue replacement, proof of consistency of biologically based scaffolds will require the development of procedures, standards, and guidelines for both procurement and assessment of biological products made from human organs and tissues. We believe that natural scaffold materials have enormous therapeutic potential and that these materials will eventually have a major impact on human health. We also feel that rigorous laboratory and clinical standards need to be formulated, which ensure that natural materials meet the specifications required for clinical application. Methods of production of acellular (AC) scaffolds and selection of decellularization reagents are important considerations since it is possible that residual cell debris or detergents could lead to induction of inflammation or development of graft rejection following transplantation. We are still at very early stages of production of biologically based scaffold materials, but design of good methods of production, cleaning, and assessment will make the shift from bench to bedside application easier and safer in the future.

We report here the first attempt to produce whole pig or human trachea-lung AC scaffolds. This is also the first use of the prototype Riddle bioreactor (Harvard Apparatus) for production of AC lung scaffolds. Postproduction assessment of the AC lung scaffolds using multiphoton microscopy (MPM) and histology indicated that the microscopic and macroscopic architecture of the pleura, distal lung borders, distal lung, bronchi, or trachea were maintained although there were changes in the density and configuration of collagen and elastin fibers due to the detergent-based decellularization process. Regardless of the extracellular matrix (ECM) changes, mechanical function of the lungs as measured by pulmonary function tests (PFTs) were similar for AC lung compared to normal lung. Postproduction assessment of cellular responses showed that stem cells and adult alveolar epithelial cells were able to attach to pig and human AC scaffolds and maintain viability. We also found that sodium dodecyl sulfate (SDS) had less of an effect on cell attachment, cell viability, apoptosis, and induction of immune responses than did other detergents currently used to produce AC natural lung scaffolds.

Materials and Methods

Procurement of lungs

For production of lung scaffolds at the University of Texas Medical Branch (UTMB), lungs were harvested from adult male Yorkshire pigs (45–60 kg) using Institutional Animal Care and Use Committee (IACUC) approved protocols and were obtained as part of a tissue sharing program. For the production of AC human lung scaffolds at UTMB, lungs were obtained as discarded human materials following a UTMB Institutional Review Board (IRB) approved protocol or at Methodist Hospital Research Institute (MHRI) following an IRB approved protocol.

For isolation of pig trachea-lungs maintained *ex vivo* at MHRI, domestic pigs (45–55 kg) were used under an experimental protocol approved by the MHRI IACUC. For the isolation of trachea-lungs at MHRI a median sternotomy was performed. Positive end-expiratory pressure (PEEP) was temporarily increased to 15–20 cm H_2O to eliminate atelectasis. A purse-string suture was placed in the main pulmonary artery (PA), which was then cannulated with a 21F arterial cannula and connected to preservation solution. The inferior vena cava and the left atrium were opened to vent the blood out. To standardize the procurement protocol for lungs we used standard procedures for human lung procurement at MHRI. In brief, pig lungs were flushed with 60 mL/kg Perfadex (Vitrolife) using gravity drainage. After Perfadex administration was complete the trachea was stapled under positive airway pressure of 20–25 mmHg. The lungs were retrieved and stored in a bag containing Perfadex solution. Human lungs were procured and treated following the same procedures described above. Pig or human lungs were examined for lung function and were then flash frozen using dry ice and stored at −80°C until use.

Ex vivo *lung perfusion*

In a subset of experiments, pig lungs were kept under static cold storage for 12 h in cold Perfadex. Trachea-lungs were transferred to the IL-16 Isolated Perfused Lung System (Harvard Apparatus). The circuit was primed with 2 L of Steen Solution (Vitrolife). The left atrial (LA) cuff was allowed to drain freely so that the LA pressure did not increase. The solution exited the pulmonary veins and was collected in a reservoir that fed the circuit and was the same solution that continued to recirculate once the system was primed. The PA cannula was attached to the donor lung PA and connected to the circuit while an endotracheal tube (8 mm inner diameter) was inserted in the trachea and secured. Flow was slowly initiated at 150 mL/min to remove air from the circuit. The temperature of the perfusate was gradually increased to 37°C. When a temperature of 32°C to 34°C was reached (usually in 20–30 min), ventilation was started using a Hamilton C-2 ventilator (Hamilton Medical, Inc.) to provide O_2 (Matheson Tri-Gas) and the perfusate flow rate was gradually increased. The solution was recirculated for the entire duration of the *ex vivo* perfusion. The flow of gas (7% CO_2, 93% N_2; Matheson Tri-Gas) through the oxygenator was used to deoxygenate and add carbon dioxide to the perfusate. Monitoring of the conditions was done using Labchart Pro Software (AD Instruments). Mean PA pressure was maintained between 10 and 15 mmHg. A protective mode of mechanical ventilation was applied with a tidal volume of 7 mL/kg at 7 bpm and PEEP of 5 cm H_2O. The lungs were expanded with inspiratory holds to an airway pressure of 20 cm H_2O every hour and pH, pCO_2, electrolytes, and glucose were maintained at physiologic concentrations in the perfusate.

Decellularization process

Organs were stored at −80°C for at least 1 month prior to decellularization. Lungs were quick thawed in a 45°C water bath and placed in the perfusion bioreactor chamber. The PA and trachea were connected to individual cannulas and separate pumping and waste systems. Two percent SDS was pumped through these cannulas and lungs were initially immersed in 2% SDS for 1 h. Lungs were then fully expanded with 1–3 L of 1% SDS solution and emptied every hour for 3 h on the first day. At the end of 3 h, the tank solution was replaced with fresh 1% SDS solution. After 12 h, 1% SDS at a rate of 100 mL/h was run through the attached cannulas from the detergent supply tank. On day 3, the flow rate was

increased to 500 mL/h. On day 7, lungs were perfused with distilled (DI) water for 12 h at a rate of 500 mL/h and was followed by phosphate-buffered saline (PBS) containing streptomycin (90 μg/mL), penicillin (50 U/mL), and amphotericin B (25 μg/mL) for 5 h at a rate of 500 mL/h. Scaffolds were then stored in the PBS, antibiotic, antimycotic solution. Tears in the pleura were repaired using fibrin glue (Baxter). For decellularization of human tissue, a cannula was attached to the main stem bronchus and PA and the single lobes were decellularized following the process described above.

Following decellularization, pieces of AC pleura, distal lung, distal lung borders, trachea, or main stem bronchus were removed to determine whether the tissue decellularization was complete or for evaluation by histochemistry, immunohistochemistry, and multiphoton imaging analysis.

Bronchoscopy protocol

Video recordings of digital bronchoscopic examination of AC lung preparations were obtained during mechanical ventilation with a tidal volume of 400 mL and PEEP of 5 mmHg. A cuffed endotracheal tube was positioned in the tracheal segment of the lung preparation and the cuff sufficiently inflated to prevent a leak during positive pressure ventilation of the preparation. A bronchoscope (Olympus model BF Type P160, Olympus Exera CVL-160 light source, and Olympus Exera CV-160 image source) was advanced into the lumen of the lung preparations through a ported double swivel elbow connected to the breathing circuit. Digital video images were recorded with a Sony model VRD-MC10 Multifunctional DVD recorder.

Pulmonary function tests

Static lung compliance measurements for normal pigs were obtained from animals being used for other UTMB IACUC studies by ventilating the lung using a patient ventilator (Model 300; Siemens-Elema) capable of measuring lung compliance. A cuffed endotracheal tube was placed in the trachea, secured with umbilical tape, and the cuff inflated to seal the tube in the trachea. The ventilator was set to deliver sufficient tidal volume to generate a peak pressure of approximately 20 mmHg. The dynamic lung compliance, peak pressures, and static lung compliance were measured using that function on the ventilator and displayed on the ventilator monitor. The screen captured image was then printed on a laser printer (Brother HL 5140; Brother International) for later analysis. PFTs of AC pig or human lung and the single human lobe were also performed as described above. PFTs obtained for the human AC lung were compared to those obtained for patients enrolled in past IRB-approved studies at UTMB.

DNA analysis

To determine whether DNA remained in the fully acellularized pig or human lung, strips of matrix were treated as previously described. Strips of AC trachea, main stem bronchus, distal lung, and pleura were digested with proteinase K and extracted with phenol–chloroform–isoamyl alcohol (25:24:1), and aqueous layers were removed and ethanol was precipitated at −20°C for 12 h to isolate any DNA present as previously described.[8] Extracted DNA for a normal lung and a deceluarized lung were run side by side along with a 5KB DNA ladder control (Invitrogen).

Immunohistochemistry

For immunostaining, cell matrix constructs or whole lungs were fixed in 2% paraformaldehyde (PAF) in PBS overnight at room temperature. Normal and AC tissues were frozen in tissue freezing medium (Triangle Biomedical Sciences) and sectioned on a Microm cryomicrotome (Thermo Scientific). Primary antibodies and dilutions used were anti-collagen I (goat 1/250; Santa Cruz Biotechnology, Inc.); anti-elastin (1/150; Santa Cruz Biotechnology, Inc.); anti-collagen IV (goat, 1/200 or 1/250; Santa Cruz Biotechnology); anti-laminin (goat, 1/200; Santa Cruz Biotechnology); and anti-fibronectin (goat, 1/250; Chemicon). For negative controls, corresponding immunoglobulin and species-matched isotype control antibodies were used, or the primary antibodies were omitted and sections were stained with secondary antibodies alone to set baseline values for analysis markers or as tissue staining controls. Secondary antibodies were conjugated to fluorescein isothiocyanate (FITC), phycoerytherin (PE), or rhodamine (Molecular Probes). Verification of cell removal was done by staining for major histocompatibility complex-1 (MHC-1) using FITC-conjugated anti-pig antibody (murine; Antigenex America, Inc.) or for the presence of human MHC-1 in human AC lung using FITC-conjugated anti-MHC-1 (murine; BD Biosciences). DNA content was evaluated using 4′,6-diamidino-2-phenylindole, dihydrochloride (DAPI) staining and was validated using gel electrophoresis.

MPM and second harmonic generation

Lung samples were imaged using MPM to detect tissue autofluorescence (AF), primarily from elastin and cells when present, and second harmonic generation (SHG) microscopy arising from fibrillar collagen.[9] MPM evaluation was done with a customized Zeiss 410 Confocal Laser Scanning Microscope modified for multiphoton excitation and detection along nondescanned optics.[10] Briefly, multiphoton excitation was from a femtosecond (fs) titanium sapphire laser (Tsunami; Spectra-Physics) having a 5W frequency-doubled Nd:YVO pump laser, and routed into the scanhead and through the sample objective. The system operated with a typical pulse width of 140 fs prior to the objective (40 × 1.2 N.A. water). An epi-configuration was used for collection of emitted light and detected using a cooled PMT placed in a nondescanned configuration (R6060; Hamamatsu). Excitation for AF was 780 nm and for SHG was 840 nm. Fluorescence emission in the spectral region of 450–650 nm was collected for detection of broadband AF from the lung. SHG was collected using a 420 ± 14 nm bandpass filter in the nondescanned detector path. The lung was placed on an imaging dish having a #1.5 coverslip and immersed in PBS. Several sites at the apex of the lobe and the bronchoalveolar region were chosen. At each site a z-stack was obtained from the outer lung surface using a z-interval of 1 μm to depths >150 μm using a 40×, 1.2 N.A. water immersion objective, which provided a field of view of 320 × 320 μm. Image reconstructions of micrograph stacks were constructed using Metamorph (Molecular Devices, Sunnyvale, CA) or Image J 3D viewer (http://rsbweb.nih.gov/ij/plugins/3d-viewer/index.html).

Use of MPM to score collagen content

The high specificity of SHG signals for fibrillar collagen enables sensitive measurements of collagen content in tissues for the purposes of quantitation.[11,12] SHG images from AC human lung were obtained from samples of bronchi, upper lung, and distal lung and images were then compared to content found in normal lung tissues at the same locations. For intensity and volume fraction scoring of SHG image stacks, three samples per category were analyzed. In each sample the SHG intensity as a function of depth first increases and then decreases due to attenuation. For intensity analysis, the 12 planes near the surface having the maximal SHG signal were selected from each imaged sample and new stacks reconstructed. Three $20 \times 20\,\mu m$ regions-of-interest (ROI) were chosen and the average intensity of each plane computed and then summed for the stack. The final intensity score was the average of each of nine total ROIs (three from each of three samples). The volume fraction measurement was carried out by taking the full stack into account. To rule out background, images were thresholded using the same threshold value on all nine image stacks. The volume fraction was then calculated as the sum of the included threshold area over the total area of all planes.

Assessment of cell adhesion to lung scaffolds

Capacity for cell attachment to AC scaffolds was examined using (1) murine embryonic stem cells (MESC), (2) human fetal lung cells (HFLC), and (3) pig bone marrow-derived mesenchymal stem cells (BMMSCs) and primary human alveolar epithelial type II cells (HAEC), which are predominately type II alveolar epithelial cells (AEC). These cell types were selected because they have either been used to produce engineered lung tissue or have been shown to adhere to natural AC lung scaffolds produced using a variety of detergents. Scaffolds that have not been well-decellularized or ones that have not been properly cleaned to remove residual detergent can exhibit low levels of cell adhesion or cell viability and high levels of apoptosis induction.

For these studies, MESCs [C57BL6 (F)] were purchased from Open Biosystems and were maintained as previously described.[8] The embryonic stem and feeder cell lines used in these studies were tested and shown to be mycoplasma negative before use. HFLCs passage 6–20, were grown in Eagle's minimum essential medium containing 10% fetal bovine serum (Intergen Co.), penicillin (100 U/mL), and streptomycin (100 μg/mL) at 37°C in a 5% CO_2 in air atmosphere. Pig BMMSCs were isolated by slicing open the tibia and scooping out the marrow using a sterile curette instrument. Bone marrow was placed in a sterile 50 cc tube filled with DMEM with penicillin (50 U/mL) and streptomycin (90 μg/mL). The tube containing bone marrow was gently shaken and then centrifuged and 2×10^6 cells per plate were cultured in a 24-well plate. Cells were cultured in DMEM with penicillin [50 U/mL] and streptomycin [90 μg/mL] and then observed for adherence to the culture dish. After 1 day nonadherent cells were removed from the plate and the remaining cells were kept in culture 4 more days. On day 5, the adherent cells were trypsinized and collected for evaluation by flow cytometry for MSC markers. Primary HAEC were collected from human lungs as previously described.[13] In brief, pieces of human distal lung were excised, chopped into $1 mm^3$ fragments, and treated with collagenase/dispase (Roche Diagnostics) for 3–5 h. Cells were collected and filtered through 100 and 40 micron filters then centrifuged to collect the AECs. Cells were cultured in small airway growth media (SAGM) (Lonza) plus 1% heat-inactivated human serum, penicillin (100 U/mL), and streptomycin (100 μg/mL) and were then incubated at 37°C and 5% CO_2. Non adherent cells were aspirated after 24 h.

Distal pig or human AC lung scaffold produced as whole trachea-lung, Matrigel and Gelfoam were cut into six equal-sized $0.5\,cm^3$ pieces and were seeded as previously described.[12] In brief, 2×10^6 MESC, HFLCs, BMMSC, or primary HAEC were suspended in 0.1 mL of Pluronic-F127 hydrogel (15% solution in DMEM) (BASF). Each cell type was injected through a 20 gage catheter into the center of each $0.5\,cm^3$ piece of AC pig or human lung, Matrigel or Gelfoam. The seeding process was followed by a 5 min centrifugation at 100 *g* to help spread cells throughout the matrix. The cell/scaffold constructs or cells alone were then placed into individual wells of a 24-well culture dish containing SAGM. Constructs were cultured at 37°C in a 5% CO_2 incubator for 24 h before placing each set of six same type cell/matrix constructs in a separate chamber of a rotary bioreactor chamber (Synthecon) for 7 days at 37°C and 5% CO_2. Cells were collected from each set of 6 cell/matrix constructs on day 7 and the total number of cells collected, number of viable cells collected, and for HAEC only, levels of cell apoptosis were also determined.

Cells were harvested from the AC matrix after 0.5 cm pieces of each cell-scaffold construct was chopped into $1\,mm^3$ fragments and treated with collagenase/dispase (Roche Diagnostics) for 30 min. Cells were collected and filtered through 100 and 40 micron filters then centrifuged to collect each specific cell type. Cells were then cultured in SAGM (Lonza) plus 1% heat inactivated human serum, penicillin (100 U/mL), and streptomycin (100 μg/mL) and were incubated at 37°C and 5% CO_2 for 2 h prior to analysis to allow for cell recovery.

Cell viability assay

Viability of the cells isolated from each cell/scaffold construct was analyzed following 7 days of culture by vital fluorescent staining (calcein-AM and ethidium homodimer-1; Molecular Probes) as previously described[8] and both live and dead cells were counted from cells isolated. The average number of live cells was calculated for each set of cell constructs grown on AC pig and AC human lung scaffold and was compared to Gelfoam and Matrigel. Cell counts were performed using a cell counter (Coulter) and percent viability was assessed by flow cytometry.

Apoptosis

Adherent cells were isolated from AC scaffolds and apoptosis was determined using TUNEL analysis as described by the manufacturer (Roche Applied Science). Apoptosis was assessed by flow cytometry.

Flow cytometry

For flow cytometry, cells were fixed with 2% PAF before analysis using a FACSAria instrument (BD Biosciences), with

acquisition and analysis using the FACSDiva program (BD Biosciences). Data from 20,000 cells were acquired for each sample.

Fluorescent microscopy

Location and extent of fluorescent labels were examined using a Nikon T300 Inverted Fluorescent microscope (Nikon Corp.). Confocal microscopy was done on a Zeiss LSM 510 UV-META confocal microscope.

Evaluation of HAEC or human immune response to AC lung scaffolds

To evaluate the HAEC or human immune cell response to scaffold produced using different detergents, a number of 2–3 cm^3 pieces of distal lung were cut from a normal human lung. Five 2–3 cm^3 pieces of lung were decellularized using 1% SDS, 0.1% SDS, 8 mM 3-[(3-Cholamidopropyl) dimethylammonio]-1-propanesulfonate (CHAPS), 0.1% triton X-100 plus 2% deoxycholate or 3% triton X-100 for 7 days followed by a 12-h DI water wash. Following decellularization of the lung tissue each 2–3 cm^3-sized piece of lung was cut into smaller 1 cm^3-sized pieces. Primary HAEC isolated from three different human donors were cultured in triplicate on 1 cm^3-sized pieces of lung for 7 days at 37°C and 5% CO_2. On day 7, the adherent cells were isolated from each piece of scaffold and the amounts for the triplicate cultures were averaged. Total cells harvested and total viable cells were determined for AC lung produced using each detergent as described above. For histological evaluation sections were stained with hematoxylin and eosin or were stained with anti-pro surfactant protein C (pro-SPC) (Santa Cruz Biotechnology) or aquaporin 5 (Pharmingen) primary antibodies followed by staining with anti-mouse FITC, PE, or Rhodamine-conjugated secondary antibodies (Molecular probes). Cells were fixed with PAF before analysis using a FACSAria instrument (BD Biosciences), with acquisition and analysis using the FACSDiva program (BD Biosciences).

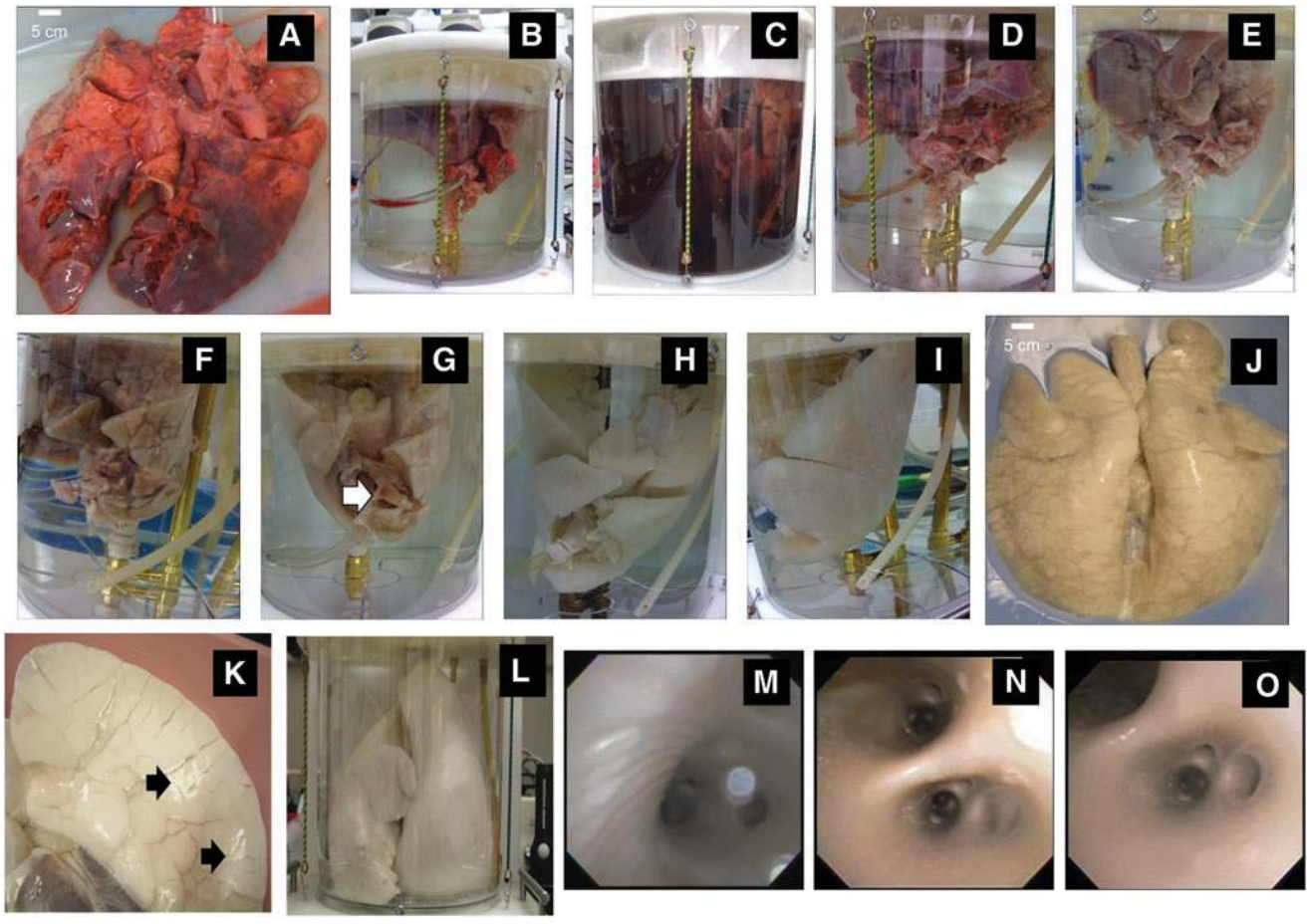

FIG. 1. Processing procedure for the decellularization of a whole pig trachea-lung. **(A)** Whole pig lung prior to processing. **(B)** Placement of cannulas into trachea and PA. **(C)** Start of decellularization process on day 1 showing discoloration of the SDS in the tank due to the presence of hemolyzed blood and cell debris. **(D)** Day 2 of process. **(E)** Day 3 of process. **(F)** Day 4 of process. Note the white regions where decellularization has taken place. **(G)** Day 5 of process. Note white arrow showing regions near the carina that have not been fully decellularized. **(H)** Day 6 of process. **(I)** Day 7 of process and **(J)** completely decellularized lung removed from tank on day 7, anterior view. **(K)** Posterior view of one lobe showing sites of fibrin glue repair of pleura (black arrows). **(L)** Lungs were expanded to examine elasticity and for PFT testing. **(M)** Bronchoscopic examination of main stem bronchus and branching airways and **(N, O)** use of same scope to view branching vessels of AC lung scaffold. SDS, sodium dodecyl sulfate; PFT, pulmonary function testing; AC, acellular; PA, pulmonary artery. Color images available online at www.liebertpub.com/tea

In a subset of experiments lung tissues were decellularized using the above detergents for 5, 7, or 14 days followed by a 12-h DI water wash. Primary HAEC were seeded onto the scaffolds in triplicate culture as described above and HAEC were isolated on day 7 and evaluated for apoptosis induction using the TUNEL assay as described above.

For examination of the human immune response, human peripheral blood was drawn from ten donors following UTMB IRB approved protocols or was isolated from whole blood purchased from UTMB blood bank. The mononuclear leukocyte (MNL) fraction was isolated as previously described using ficoll-hypaque (GE Healthcare).[14,15] MNLs were not labeled or were labeled with carboxyfluorescein succinimidyl ester (CFSE; Molecular Probes)[8] prior to incubation in triplicate culture with human AC lung produced using the detergents listed above. Three $0.5\,mm^3$-sized pieces of each detergent-treated human AC lung scaffold were incubated with 2×10^6 CFSE labeled MNL in a separate well of a 24-well tissue culture plate (Corning) for 5, 7, or 14 days at 37°C and 5% CO_2. At the end of each culture period the MNLs in each triplicate culture were collected and cells were stained with 20 ul of anti-CD3 PE (BD Biosciences) to identify CD3-positive T cells in the culture. Following CD3 cell staining all samples were fixed in 2% freshly made PAF until they were analyzed by flow cytometry.

Chemokine production was measured in MNL cultures that were not CFSE labeled. In these experiments, 2×10^6

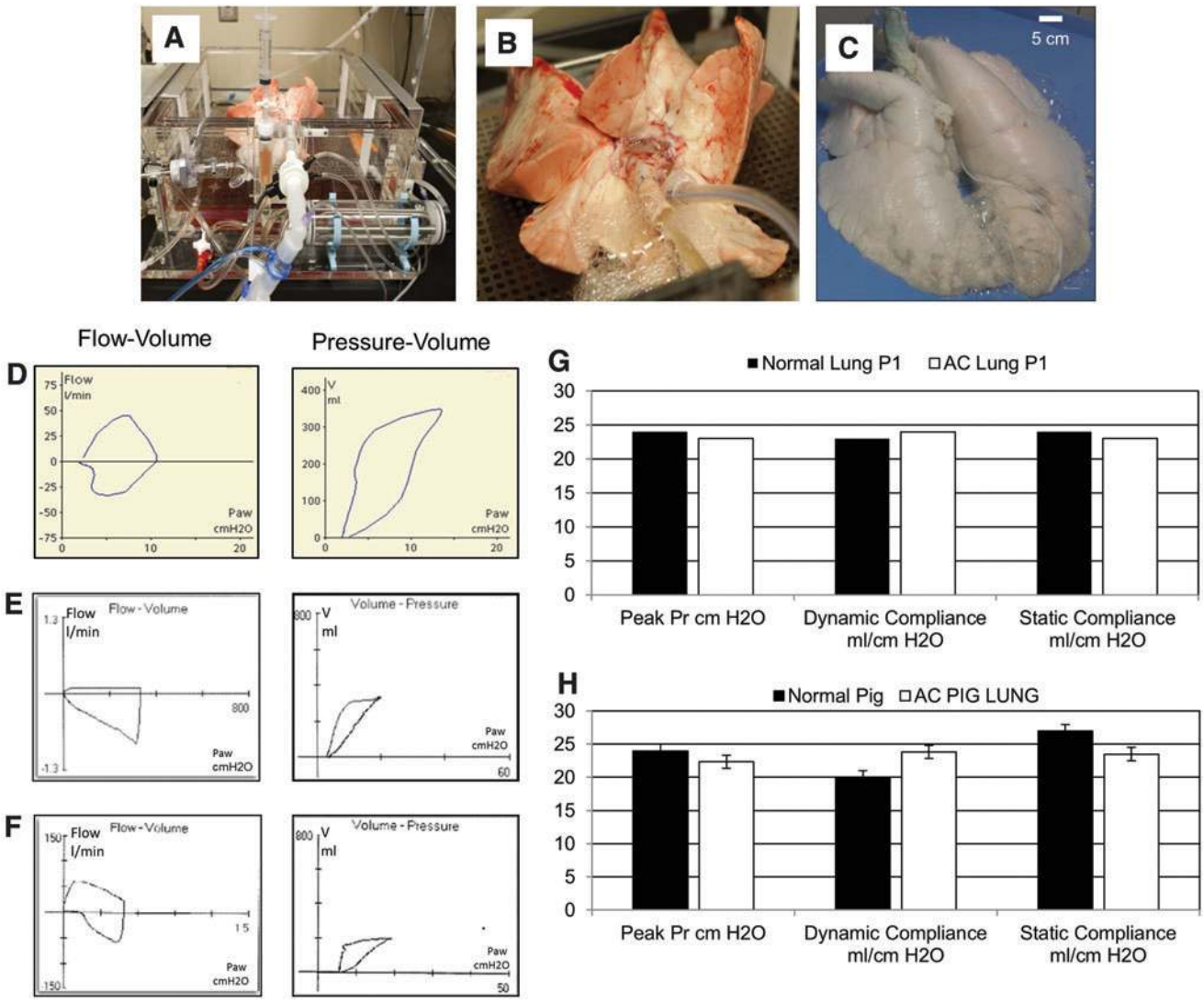

FIG. 2. Evaluation of mechanics of lung function **(A)** Harvard Apparatus-ventilator system supporting a whole pig lung. **(B)** Close-up image of pig lung in panel **(A)** showing placement of endotracheal tube and cannula into PA. **(C)** Whole AC pig lung attached by endotracheal tube to ventilator. **(D)** Measurements of flow-volume loop (left) and pressure-volume loop (right) for lung shown in panels **(A)** and **(B)** above. **(E)** Measurement of flow-volume loop (left) and pressure-volume loop (right) for AC pig lung shown in panel **(C)**. **(F)** Measurements of flow-volume loop (left) and pressure-volume loop (right) for live pig being maintained on a ventilator. **(G)** Representative examination of the peak pressure, dynamic compliance, and static compliance for a single pig lung pre (■) and post (□) decellularization. **(H)** Averaged data for peak pressure, dynamic compliance, and static compliance for $n=8$ pig lungs measured pre (■) and post (□) decellularization. Color images available online at www.liebertpub.com/tea

MNLs from each donor were cultured in triplicate with 0.5 mm^3 pieces of AC lung scaffold produced using the detergents listed above. Constructs were cultured in a 24-well plate containing SAGM at 37°C and 5% CO_2. At the end of 5 days, cell culture supernatants were removed and production of chemokines CXCL8/IL-8, CCL5/RANTES, CXCL9/MIG, and CXCL10/IP-10 was assessed using a Cytometric Bead Array human chemokine kit as described by the manufacturer (BD Biosciences) on a FACSort flow cytometer (BD Biosciences).

Statistical analysis

Statistical analysis was performed using GraphPad InSTAT software (version 2003). Mean values and standard deviation are reported. Analysis of variance (ANOVA) was performed and data was subjected to Tukey–Kramer multiple comparison test. Mean differences in the values were considered significant when p was less than 0.05.

Results

Quick thawing followed by slow infusion of SDS through the trachea and PA maximized the disruption of cells and facilitated removal of cell debris from the lung. Figure 1A–J document the process of decellularization from start (Fig. 1A) to finish (Fig. 1J). Figure 1B shows the placement of the PA cannula and the attachment of the trachea to the bioreactor. Within the first few hours of processing the tank fluid became dark due to the presence of blood and cell debris (Fig. 1C). After 2–3 days the distal-most regions of the pig lung turned white (Fig. 1D, E). Distal lung was becoming decellularized by day 4 (Fig. 1F). By day 5 only a few small areas in the internal regions of the lung retained cell debris

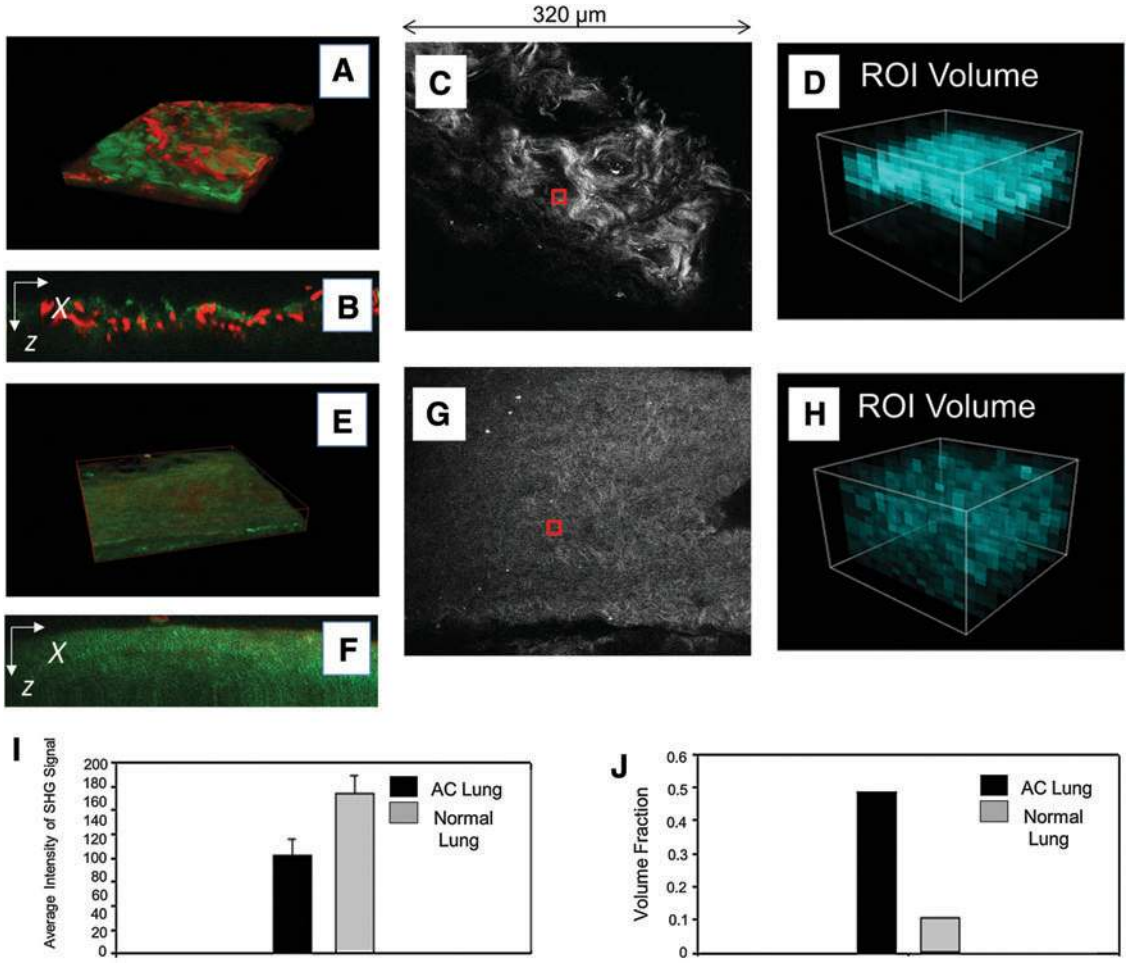

FIG. 3. MPM-SHG scoring of pig normal versus AC lung. **(A)** MPM 3D reconstruction image of normal lung ECM using SHG to image collagen (green) and AF for elastin (red). **(B)** Single XZ cross section of A. **(C)** A scored ROI (red box) is shown for normal pig lung. **(D)** Volumetric representation of the distribution of the collagen SHG intensity of the region denoted by red box in **(C)**. **(E)** MPM 3D reconstruction image of AC pig lung ECM using SHG to image collagen (green) and AF for elastin (red). **(F)** Single XZ cross section of **(E)**. **(G)** A representative scored ROI (red box) is shown for AC pig lung. **(H)** Volumetric representation of the distribution of the collagen SHG intensity of the region denoted by red box in **(G)**. **(I)** Averaged scoring results for normal versus AC lung based on the average of the SHG intensity from each case. **(J)** Volume fraction of the SHG signal in normal versus AC lung showing that although the intensity of SHG is higher in the native lung, the distribution of collagen is more uniform in the AC lung. MPM, multiphoton microscopy; AF, autofluorescence; SHG, second harmonic generation; ECM, extracellular matrix; ROI, region of interest; 3D, three-dimensional. Color images available online at www.liebertpub.com/tea

(Fig. 1G, white arrow). On day 6 (Fig. 1H) decellularization was almost complete. A fully decellularized AC whole pig scaffold was produced by day 7 (Fig. 1I–K). Although there were some pleural tears on the distal side of the pig lung (Fig. 1A) the remainder of the lung was intact and tears were easily sealed with fibrin glue (Fig. 1K, arrows). Once repaired the pleural tears did not inhibit inflation of the lung (Fig. 1L) or subsequent PFT measurements. Bronchoscopy of blood vessels and lung airway indicated that macroscopically the underlying gross structures and branching of both airway (Fig. 1M) and (Fig. 1N, O) vessels remained intact after decellularization with no evidence of gross structural damage, sloughed cell material, or cell debris.

A freshly isolated pig lung maintained in a Harvard apparatus system (Fig. 2A, B) or an AC pig lung (Fig. 2C) are shown. PFTs of excised pig lungs maintained *ex vivo* (Fig. 2D) or AC lungs (Fig. 2E) were similar to those for live ventilated pigs (Fig. 2F). Representative measurements for lungs from one pig show a comparison between PFTs of normal pig lung and the same set of lungs following decellularization (Fig. 2G). Averaged PFT values for lungs obtained from $n=8$ pigs pre- and post decellularization indicated that AC lungs did not exhibit statistically relevant changes in peak pressure, dynamic compliance, or static compliance when compared to normal pig lungs (Fig. 2H).

Immediately after PFT evaluation pieces of pig AC pleura, distal lung, distal lung borders, trachea, or main stem bronchus were removed for histological and MPM analysis. MPM was used to examine the effects of the decellularization process on anatomical components of the lung, which we considered essential to the production of AC lung scaffolds. MPM was also used to evaluate the decellularization process using AF to measure the presence of cells or cell debris. MPM measurements of SHG were used to examine collagen content in normal pig lung (Fig. 3A–D) and AC pig lung (Fig. 3E–H). MPM SHG ROIs were used to quantitate collagen content in the AC pig lung and are shown for normal (Fig. 3C, D) and AC pig lungs (Fig. 3G, H). Averaged volume density analysis, the intensities of all ROIs from each plane of the stacks indicated that AC pig lung contained half the amount of collagen as normal lung (Fig. 3I) and volume fractions measured were twice the level of AC versus normal lung (Fig. 3J) as expected based on the volume fraction measurements. Comparison of the ROIs (Fig. 3D vs. 3H) indicated that normal pig lung contained higher levels of collagen than AC lung. Regardless of the reduction in collagen content the gross macroscopic and microscopic structures of the pig lung were retained in the AC lung scaffold. MPM images of collagen and elastin of normal pig lung (Supplementary Fig. S1A–H; Supplementary Data are available online at www.liebertpub.com/tea) and regions of AC pig trachea are presented as Supplementary Figure S2A–G.

ECM of pig AC pleura (Fig. 4A–F and G–J) and distal lung (Fig. 5A–P) were predominately composed of collagen type-I and elastin. Although the AC distal lung was shown to

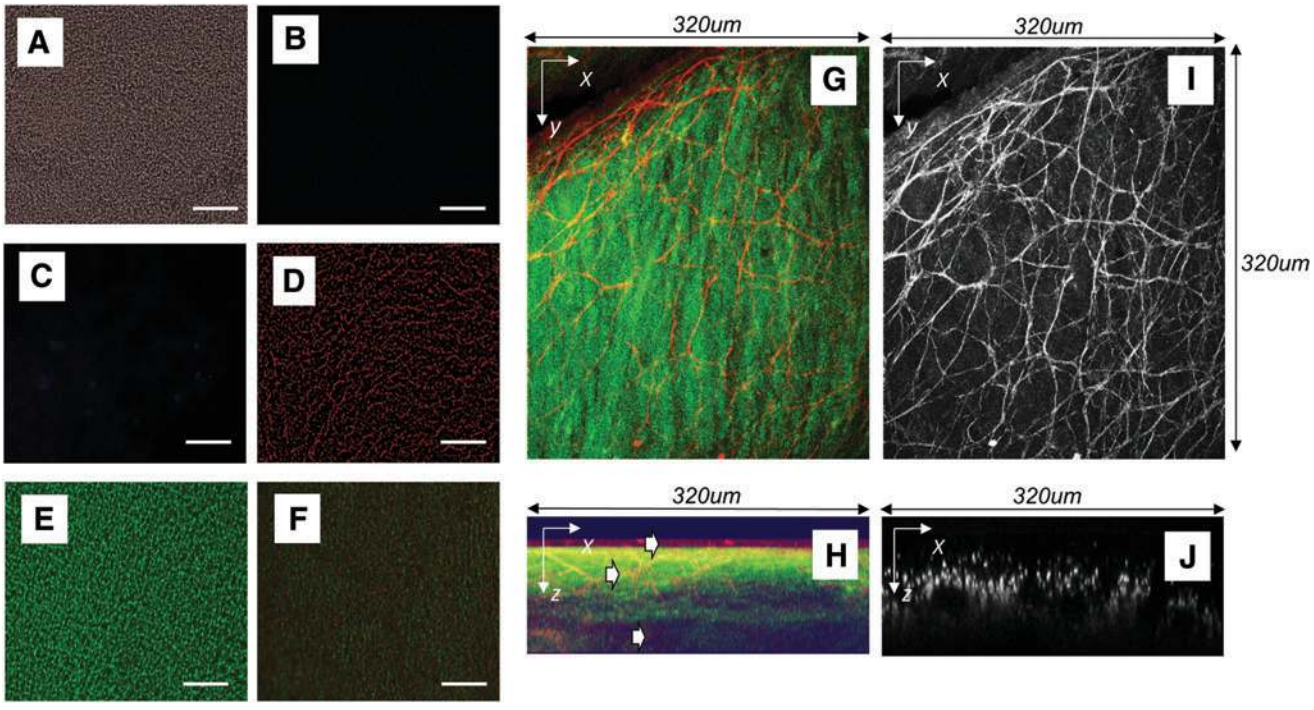

FIG. 4. Evaluation of AC pig pleura. **(A)** Phase contrast microscopic image of AC pig pleura, scale bar = 100 μm. **(B)** Evaluation of presence of nuclei, nuclear material using DAPI, or cell debris by staining for pig MHC-1, scale bar = 100 μm. **(C)** Staining control for **(D)** and **(E)**. **(D)** Staining for presence of elastin (red) and **(E)** Collagen (green), scale bar = 100 μm. **(F)** Merge of **(B)** and **(D)**, scale bar = 100 μm. **(G)** MPM image of pleura using combined AF of elastin (red) and SHG of collagen (green). **(H)** 90° (XZ) cross-sectional view of **(G)**. White arrows indicate elastin fibers between collagen bands. **(I)** MPM AF image of pleura using MPM showing bright elastin fibers. **(J)** Single XZ cross section of I showing depth-resolved structure obtained by AF. DAPI, 4′,6-diamidino-2-phenylindole, dihydrochloride; MHC, major histocompatibility complex-1. Color images available online at www.liebertpub.com/tea

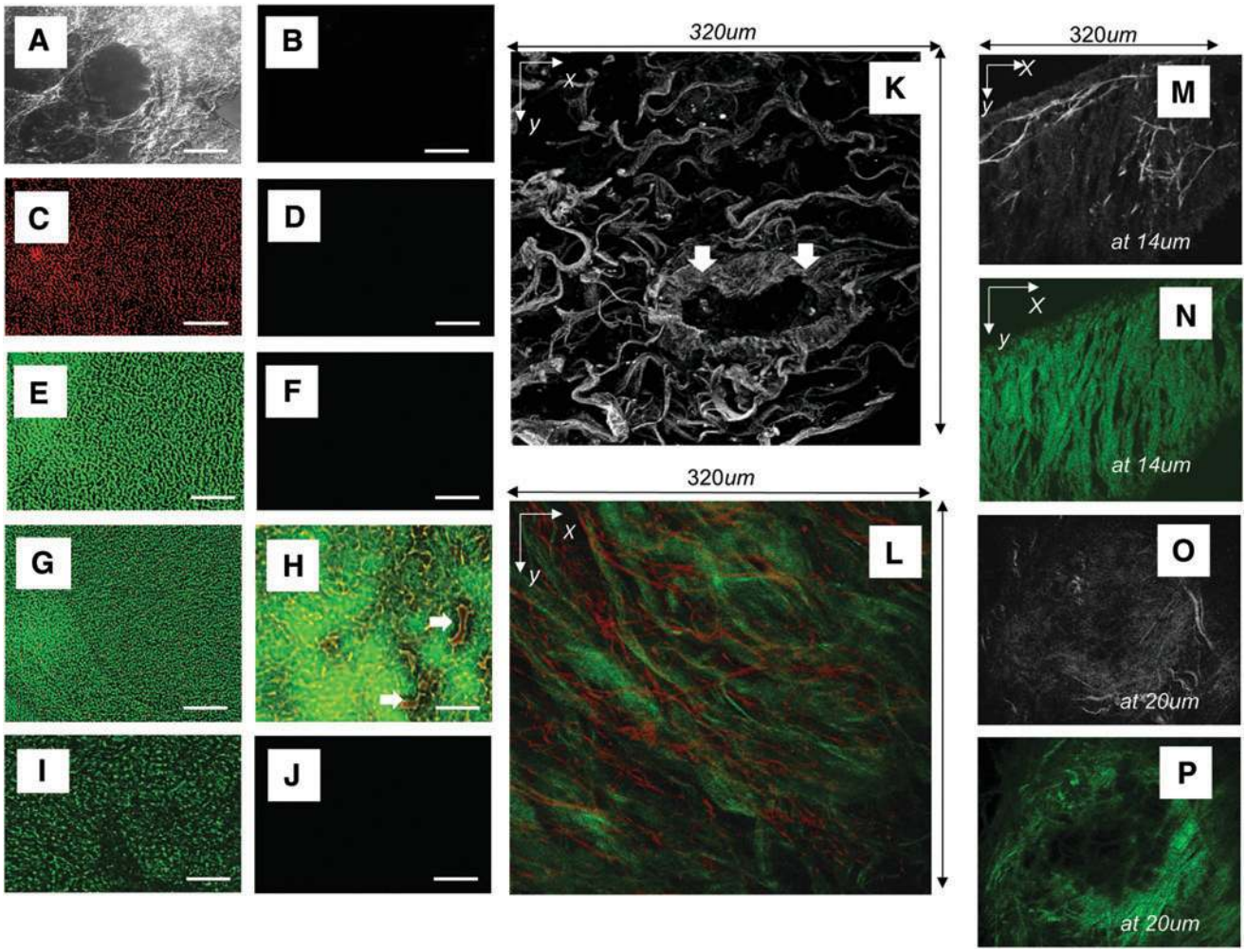

FIG. 5. Evaluation of AC pig distal lung. **(A)** Phase contrast microscopic image of AC pig distal lung, scale bar = 100 μm. **(B)** Evaluation of presence of nuclei, nuclear material using DAPI, or cell debris by staining for pig MHC-1. **(C)** Staining for presence of elastin (red), scale bar = 100 μm. **(D)** Staining control for **(C)**. **(E)** Staining for the presence of collagen (green), scale bar = 100 μm. **(F)** Staining control for **(E)**. **(G)** Merge of **(C)** and **(E)**, scale bar = 100 μm. **(H)** Merge of section stained for elastin (red) and collagen (green) showing that ECM of small blood vessels remains intact, scale bar = 100 μm. White arrows point to blood vessels in AC distal lung. **(I)** Staining for presence of fibronectin (green), scale bar = 10 μm. **(J)** Staining control for **(I)**. **(K)** MPM images of distal lung using AF for elastin. White arrows point to ECM of a blood vessel in cross section. **(L)** MPM z-projection of distal lung using combined AF and SHG showing elastin fibers (red) and bundles of collagen (green) imaged to a depth of 140 μm. **(M, N)** Border of AC distal lung using AF at a depth of 14 μm at edge of distal lung indicating high elastin content. **(M)** Bright elastin fibers amid lower intensity collagen (grey background), and **(N)** corresponding SHG of same area in panel **(M)** showing the signal specific to bundles of collagen fibers (green). **(O)** MPM AF at a depth of 20 μm of small bronchiole showing bright elastin fibers and gray background (collagen). **(P)** SHG of same area in **(O)** showing bundles of collagen fibers (green). Color images available online at www.liebertpub.com/tea

contain fibronectin (Fig. 5I) AC pleura did not (data not shown). Laminin and collagen IV were also not retained in the AC pig pleura, distal lung, trachea, or bronchi (data not shown). The gross configurations of the layers of elastin and collagen that make up the pleura in AC pig lung were retained after decellularization of the lung (Fig. 4F, G–J). Elastin fibers that extend between bands of collagen layers also remained (Fig. 4H). MPM using AF allowed for visualization of the interconnections of elastin fibers forming a net-like configuration over the lung (Fig. 4G–J).

AC pig distal lung in the relaxed state was formed of a loose network of fibers (Fig. 5A) and was shown to contain no cells or cell debris by MHC class-1 staining (Fig. 5B) or MPM AF (Fig. 5K, M–P). There were small amounts of elastin (Fig. 5C, G, H) but high levels of collagen I (Fig. 5E, G, H) and fibronectin (Fig. 5I). The white arrows in Figure 5H and K point to the remaining AC ECM of small blood vessels in the distal lung. Vessels contained inner layers of elastin (Fig. 5H, K), which were surrounded by thick bundles of collagen (Fig. 5H, K). Normal pig lung (Supplementary Figs. S1 and S2) and distal regions of AC lung scaffold (Fig. 5L) both contained thick bundles of collagen interlaced with elastin. The collagen fibers in normal lung had a wavy appearance (Supplementary Fig. S2) while fibers in AC lung had a more relaxed configuration (Fig. 5K–N).

The prototype Riddle bioreactor containing an adult trachea-lung is shown in Figure 6A. The lung is suspended from the bottom of the tank and a white arrow points to the row of peristaltic pumps used to supply detergent to the PA, trachea, and bioreactor chamber. Gross images of human lungs post decellularization are shown (Fig. 6B, C). Bronchoscopy of blood vessels and lung airway indicated that macroscopically the underlying gross structures and branching of airway (Fig. 6D, E) and vessels (Fig. 6F, G) remained intact after decellularization with no evidence of cell debris or structural damage.

The AC human lungs were expanded after placement of an endotracheal tube into the trachea or main stem bronchus (Fig. 6B, C). PFT flow-volume (left) and volume-pressure loops (right) were shown for a normal individual maintained on a respirator from a past UTMB IRB-approved study (Fig. 6H) and for the AC human trachea-lung (Fig. 6I). Flow-volume and pressure-volume loops from $n=6$ human lungs pre- and postdecellularization (Fig. 6J) were not found to be significantly different for normal compared to AC human lung. Initial opening pressures were increased in the AC lungs due to the presence of residual liquid (PBS) or perhaps due to lack of surfactant in the AC scaffold.

Normal human lung (Supplementary Fig. S3A–E and Fig. 7A, B) and AC human lung (Figs. 7E, F and 8K, L), bronchus (Supplementary Fig. S4A–F), and pleura (Supplementary Fig. S5A–J) were imaged using MPM. MPM SHG was used to examine collagen content in normal (Fig. 7A–D) and AC human lung (Fig. 7E–H). A representative MPM SHG ROI used to quantitate collagen content is shown for normal (Fig. 7C) and AC human lung (Fig. 7G). Averaged volume density analysis, the intensities of all ROIs from each plane of the stacks, indicated that AC human lung contained half the amount of collagen as normal lung (Fig. 7I) and volume fractions measured were greater for AC versus normal human lung (Fig. 7J).

Despite the loss of collagen, gross macroscopic and microscopic lung structures were retained in human lung following decellularization (Fig. 8 and Supplementary Figs. S4 and S5). MPM analysis did not indicate the presence of cellular debris in the regions examined (Fig. 8K, L and Supplementary Figs. S4 and S5). The AC human distal lung had

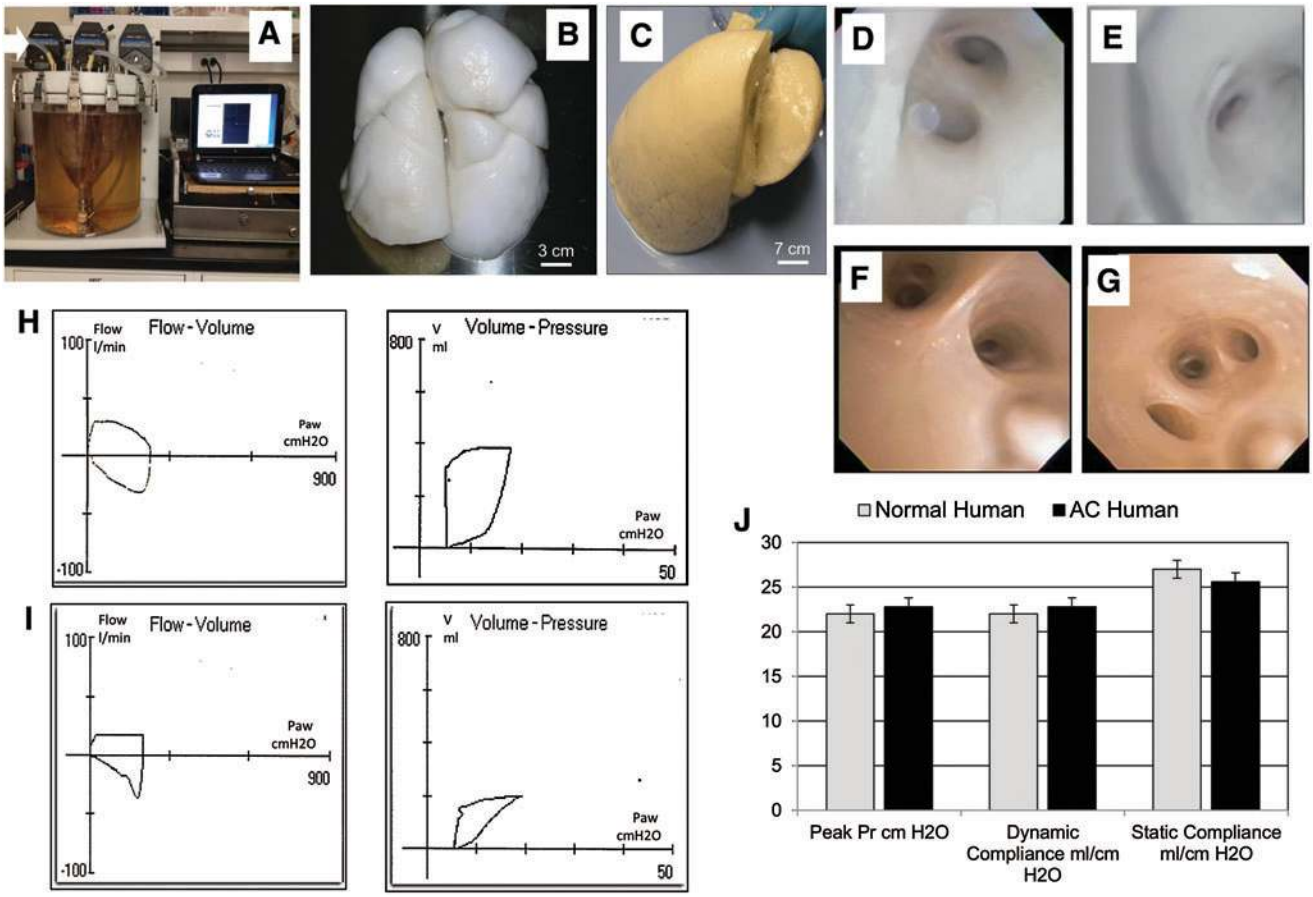

FIG. 6. Production and evaluation of AC human trachea-lung. **(A)** Image of bioreactor containing an adult trachea-lung. **(B)** Gross image of an AC pediatric trachea-human lung and **(C)** AC main stem bronchus and lobe of an adult lung. **(D, E)** Bronchoscopic views imaged through right main stem bronchus of the adult AC lobe in panel **(C)** showing the branching airway. **(F, G)** Use of a bronchoscope to view the PA showing branching of blood vessels. **(H, I)** PFTs showing **(H)** normal human ventilation profiles with flow-volume loop (left) and volume-pressure loops (right). **(I)** PFTs of AC human lung showing ventilation profiles and flow-volume loop (left) and volume-pressure loops (right). **(J)** Averaged data for peak pressure, dynamic compliance, and static compliance for $n=6$ adult human lungs measured pre (■) and post (□) decellularization. Color images available online at www.liebertpub.com/tea

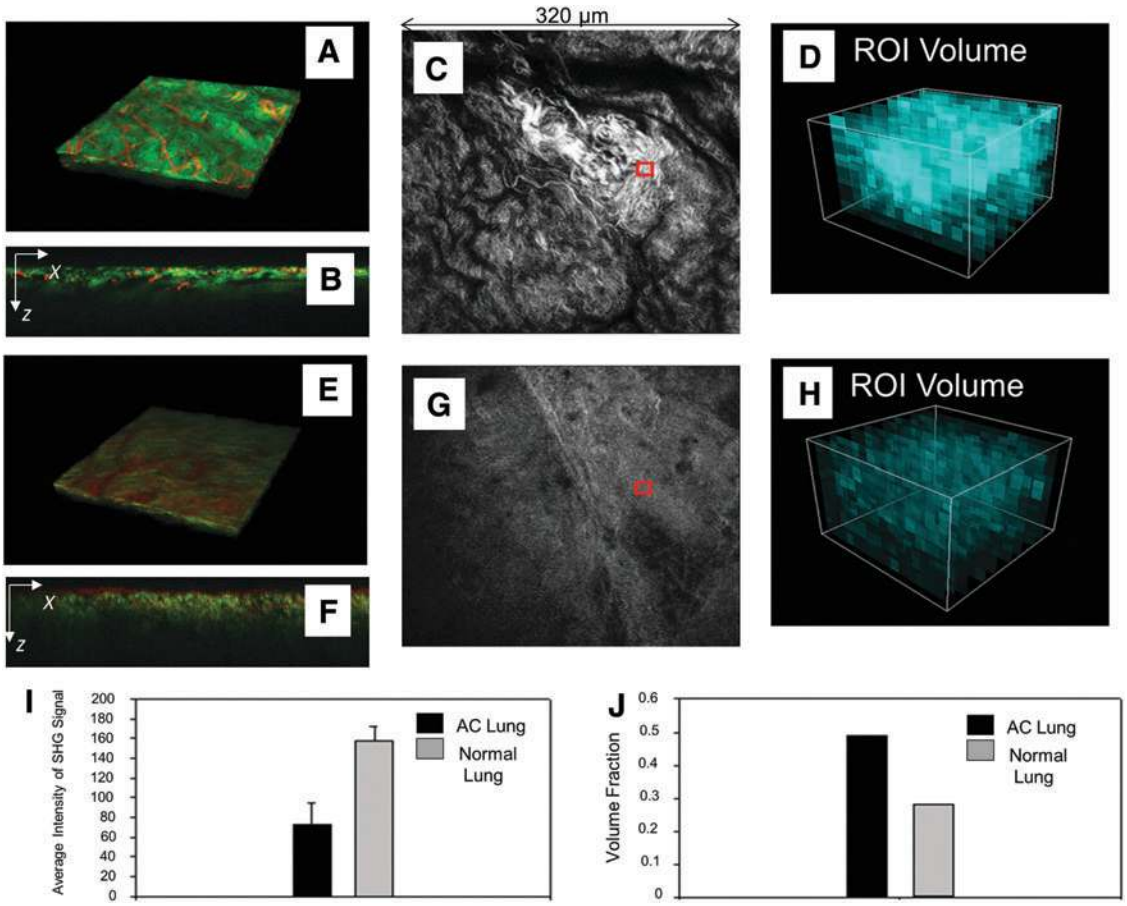

FIG. 7. MPM-SHG scoring of human normal versus AC lung. MPM evaluation of normal lung **(A–D)**. **(A)** MPM 3D reconstruction image of normal lung ECM using SHG to image collagen (green) and AF for elastin (red). **(B)** Single XZ cross section of **(A)**. **(C)** SHG to visualize collagen of normal lung. A scored ROI (red box) is shown. **(D)** Volumetric representation of the distribution of the collagen using SHG intensity of the region denoted by red box in **(C)**. **(E–H)** MPM evaluation of AC lung. **(E)** MPM 3D reconstruction image of AC human lung using SHG to image collagen (green) and AF for elastin (red). **(F)** Single XZ cross section of E. **(G)** SHG was used to visualize collagen. A scored ROI (red box) is shown for AC human lung. **(H)** Volumetric representation of the distribution of the collagen SHG intensity of the region denoted by red box in **(G)**. **(I)** Averaged scoring results for normal versus AC lung based on the average of the SHG intensity from each case. **(J)** Volume fraction of the SHG signal in normal versus AC lung showing that although the intensity of SHG is higher in the native lung, the distribution of collagen is more uniform in the AC lung. Color images available online at www.liebertpub.com/tea

a loose arrangement of fibers (Fig. 8A) and contained no nuclei or DNA (Fig. 8B, J). Immunostaining revealed that the distal lung contained dense bundles of collagen with small amounts of interlaced elastin fibers (Fig. 8C, E, G). Fibronectin could also be found in all of the areas evaluated in distal lung (Fig. 8I) but no cells or cell debris was present as measured by staining for human MHC-1 (Fig. 8H) or as indicated by AF in the MPM analysis (Fig. 8K, L).

The decellularized human main stem bronchus retained its shape and structure (Supplementary Fig. S4A). The lacunae in the cartilage rings contained no cells, nuclei or nuclear material (Supplementary Fig. S4B–D). MPM examinations of human AC bronchus showed a parallel configuration of collagen I and elastin was present (Supplementary Fig. S4E, F) similar to what was found in AC pig lung (Supplementary Fig. S2).

Postproduction assessment of DNA isolated from trachea, main stem bronchus, distal lung, and the pleura of human lungs indicated that the 1% SDS treatment removed even low molecular weight fragmented DNA. A single representative DNA assessment for one lung pre- and post decellularization is shown in Figure 9A.

Post production lung construct assessment for attachment of cells to pig AC lung or human AC lung was done. MPM images of MESC cultured on AC pig lung scaffold showed that cells (in red or designated by white arrows) adhered to the pig AC scaffold (Fig. 9B, C) in a manner similar to normal tissue (Fig. 9D). All cell types evaluated were found to attach to the AC pig scaffold (Fig. 9E, H, K). Few cells attached to Gelfoam (Fig. 9F, I, L) or Matrigel (Fig. 9G, J, M). Averaged data for counts of total cells and viable cells harvested from cell/scaffold constructs for MESC (Fig. 9N), pig BMMSCs (Fig. 9O), HFLC (Fig. 9P), and primary HAEC (Fig. 9Q) indicated that viability and retention of cells was greater for cells cultured on AC pig or AC human scaffolds regardless of the cell source used to populate the matrix, and there were significantly more viable cells on the AC natural matrix (pig or human) than on either Gelfoam ($p<0.05$) or Matrigel

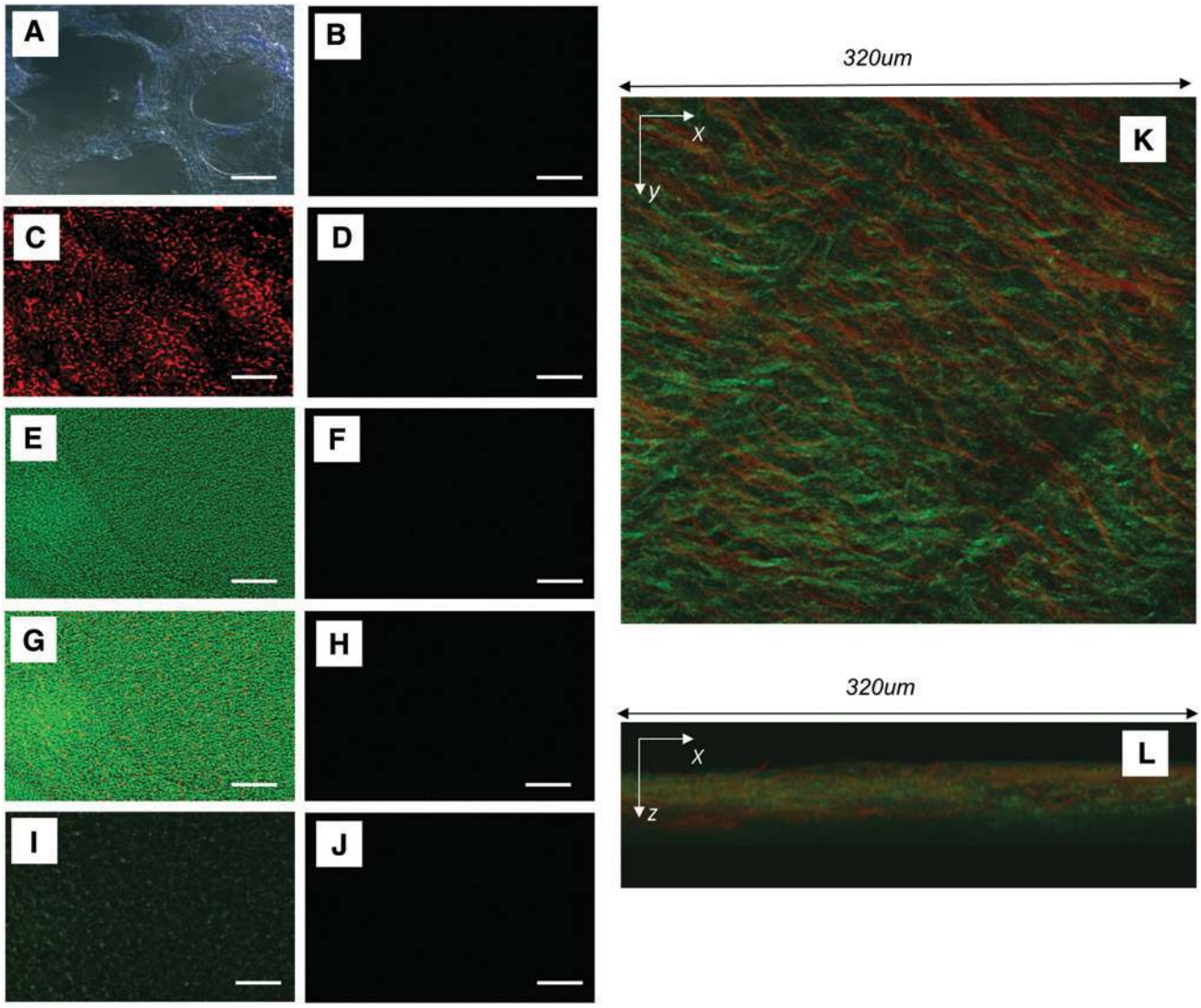

FIG. 8. Evaluation of AC human distal lung. **(A)** Phase contrast microscopic image of AC distal lung, scale bar = 100 μm. **(B)** Evaluation of presence of nuclei and nuclear material using DAPI. **(C)** Staining for presence of elastin (red), scale bar = 100 μm. **(D)** Staining control for C. **(E)** Staining for presence of collagen (green) and cell nuclei using DAPI (blue), scale bar = 100 μm. **(F)** Staining control for **(E)**. **(G)** Merge of **(C)** and **(E)**, scale bar = 100 μm. **(H)** Evaluation of cell debris using staining for human MHC-1 (green) in AC distal lung, scale bar = 100 μm. **(I)** Staining for fibronectin (green), scale bar = 100 μm. **(J)** Staining control for **(I)**. **(K)** MPM images of distal lung using combined AF with SHG for elastin (red) and collagen (green). **(L)** 90° (XZ) cross-sectional view of **(K)**. Color images available online at www.liebertpub.com/tea

($p < 0.05$) after 7 days of culture. There were no significant differences in numbers of viable cells obtained from AC pig or AC human lung scaffolds. Culture of primary HAEC on tissue culture plates yielded significantly fewer total and fewer viable cells than did culture on the three-dimensional (3D) AC lung scaffolds (Fig. 9Q) ($p < 0.05$). Primary HAEC attached well to AC human scaffolds produced using 1% SDS (Fig. 10A–I) and H & E staining or immunostaining showed that cells covered most of the scaffold surface. Initially, HAEC attached in clumps (Fig. 10C, D) and then slowly spread out over 7 days of culture (Fig. 10F–H). The HAECs at isolation and after 1 day of culture predominately expressed pro-SPC (Fig. 10G) indicating that as expected most were AEC II but over time some small pockets of cells were shown to be AQ5 positive (Fig. 10H). Total adherent cells collected and viability of primary HAEC on human lung scaffolds produced using a variety of detergents was only significantly different for scaffolds made using 8 mM CHAPS or 0.1% triton X-100 followed by 2% sodium deoxycholate ($p < 0.05$) (Fig. 11A). Apoptosis of primary HAEC was lowest for 1% SDS scaffolds produced after 5, 7, or 14 days of decellularization processing ($p < 0.05$) but was not significantly different for scaffolds produced after 14 days of processing using 3% triton X-100 (Fig. 11B).

T cell activation and chemokine production was evaluated by culturing human MNLs from 10 blood donors with AC human scaffold produced using a variety of detergents. Results from both T cell activation assays measuring CFSE loss (Fig. 12A), or production of chemokines involved in inflammation or graft rejection (CCL5, CXCL9, CCL2, or

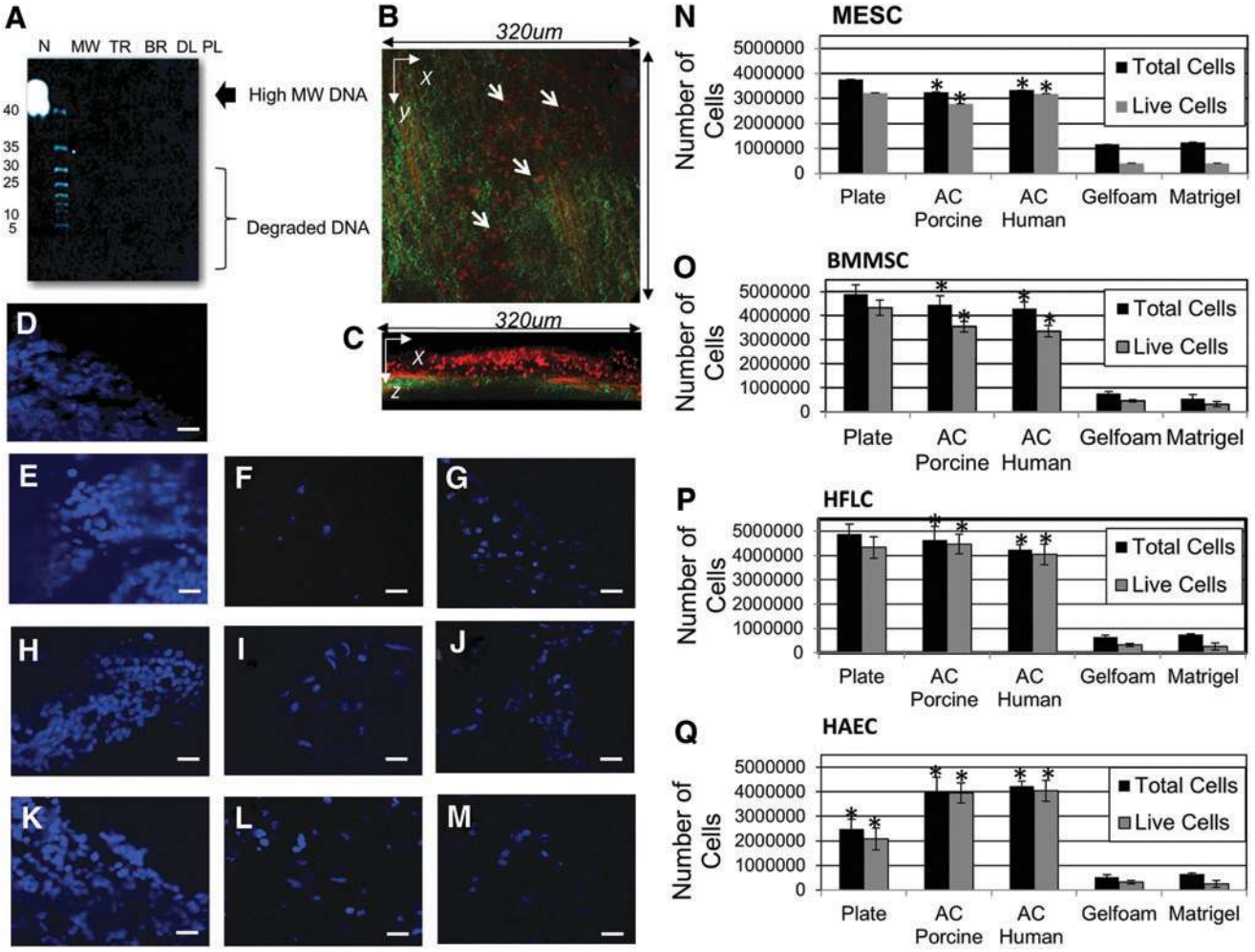

FIG. 9. Post production DNA content evaluation and assessment of cell viability. **(A)** Evaluation of residual DNA in a normal human lung pre-decellularization and for one representative human lung post decellularization. **(B)** MPM z-projection of distal recellularized AC Pig lung showing AF arising from elastin fibers and cells (red) and SHG from collagen (green). Cells are also designated by white arrows. **(C)** 90° (XZ) cross-sectional view of **(B)**. Note cells (red) attached to the ECM. **(D)** DAPI staining of normal lung. **(E, F, G)** DAPI staining of MESC nuclei (blue) cultured for 7 days or cells cultured on **(E)** AC pig lung scaffold, **(F)** Gelfoam or **(G)** Matrigel. **(H, I, J)** DAPI staining of HFLC nuclei (blue) cultured on **(H)** AC pig lung, **(I)** Gelfoam or **(J)** Matrigel. **(K, L, M)** DAPI staining of nuclei of pig BMMSC cultured on **(K)** AC pig lung, **(L)** Gelfoam or **(M)** Matrigel. **(N–Q)** Averaged data for evaluation of total number of cells and number of viable cells harvested at 7 days from each scaffold material. Average number of total cells and viable cells at 7 days for **(N)** MESC, **(O)** BMMSC, **(P)** HFLC, or **(Q)** HAEC after culture on AC pig lung, AC human lung, Gelfoam or Matrigel scaffolds. Both AC pig lung and AC human lung had significantly more cells and viable cells at 7 days of culture than either Gelfoam or Matrigel ($^*p < 0.05$). HAEC AC pig and AC human scaffold constructs also yielded significantly more intact primary HAEC and more viable HAEC than plate culture ($^*p < 0.05$). MESC, murine embryonic stem cells; BMMSC, bone marrow-derived pig mesenchymal stem cells; HFLC, human fetal lung cells; HAEC, human alveolar epithelial type II cells. Color images available online at www.liebertpub.com/tea

CXCL-10) (Fig. 12B), indicated that scaffold produced after 7 days of processing in 1% SDS was significantly less immunogenic ($p < 0.05$) than scaffolds produced using 0.1% SDS, 8 mM CHAPS, and 0.1% TritonX-100 followed by sodium deoxycholate but not 3% triton X-100.

Discussion

Synthetic and natural scaffolding materials including AC natural mouse or rat lung have been used to engineer lung tissue with mixed results.[16–27] One of the most logical and intuitive ways to look for alternatives to solid biodegradable scaffold-based tissue engineering approaches is to use the decellularized matrix of the organ that needs to be replaced.[28] Natural scaffolds possess the organ-specific shape and size appropriate for surgical implantation. This approach also exploits the organ-specific structural, microscopic, and macroscopic organization of ECM necessary to support the mechanical process of breathing, which are maintained in the AC lung scaffold.[28]

The ultimate aim of this work was to examine the feasibility of developing a large whole-organ lung scaffold. Studies utilizing natural AC lung scaffolds produced from lungs obtained from mice or rats have shown that engineered lung

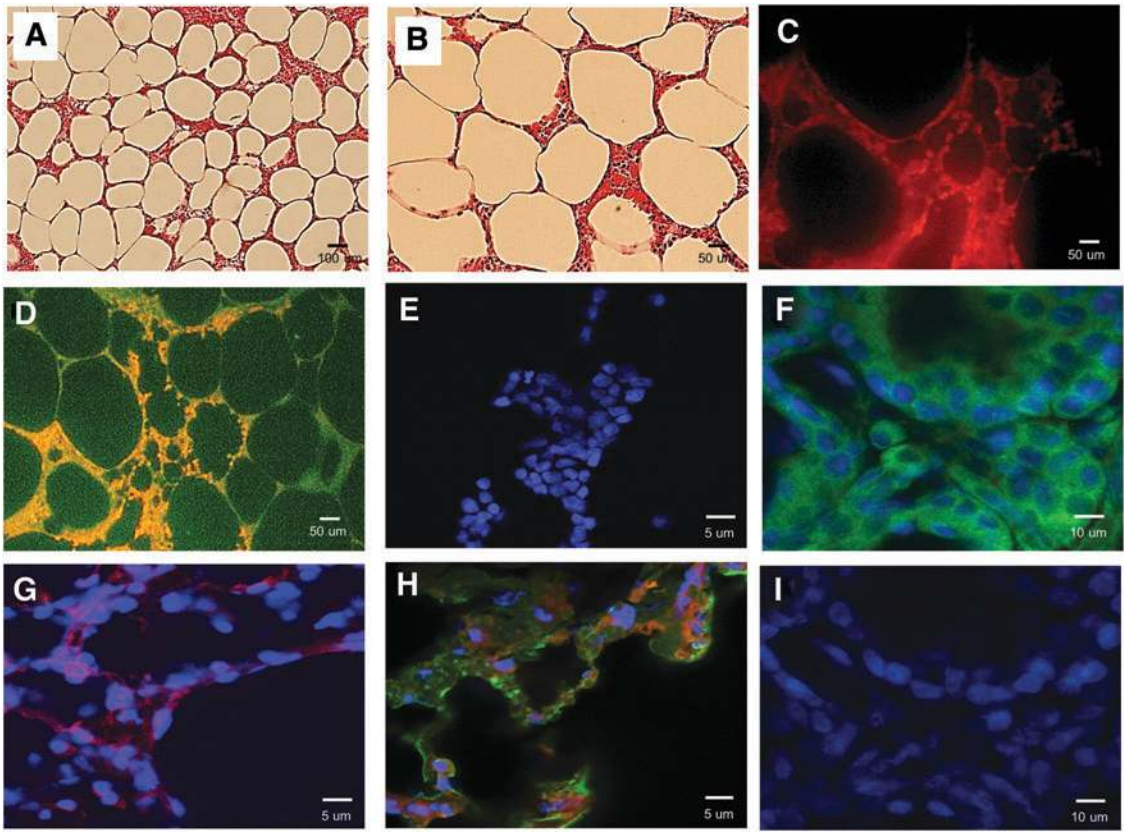

FIG. 10. Human alveolar epithelial cell culture **(A)** H&E of HAEC cultured for 7 days on AC human lung, scale bar = 100 μm. **(B)** H& E of HAEC cultured for 7 days on AC human lung, scale bar = 50 μm. **(C)** Examination of section of HAEC on human lung, day 1 post seeding of cells, stained to show pro-SPC (red). Scale bar = 50 μm **(D)** Examination of section of HAEC on human lung, day 1 post seeding of cells, stained to show pro-SPC (red) showing cell adhesion on portions of scaffold. Scale bar = 50 μm **(E)** Staining control for panel **(F)**. Scale bar = 5 μm. **(F)** Examination of section of HAEC on human lung, 5 days post seeding of cells, stained to show pro-SPC (green). Scale bar = 10 μm. **(G)** Examination of section of HAEC on human lung, 7 days post seeding of cells, stained to show pro-SPC (red). Scale bar = 5 μm. **(H)** Section of HAEC on AC human lung scaffold, 7 days post seeding of cells, stained to show pro-SPC (green) and aquaporin 5 (red). Scale bar = 5 μm. **(I)** Staining control for **(C–H)**. Scale bar = 10 μm. pro-SPC, pro surfactant protein C. Color images available online at www.liebertpub.com/tea

tissues can be grown on these small AC natural lung scaffolds regardless of the detergent or methods used to produce them.[12,23–27] In a few cases engineered lungs were transplanted into animal models with limited ability to support gas exchange.[25–27] Although AC scaffolds do not possess any normal cellular components that allow breathing and air exchange to occur they do provide key ECM components that support its mechanical functions as indicated by the near-normal PFT values in these small animal studies.[24–27] Little work has been done to assess the feasibility of producing large organs such as those obtained from pigs or humans. We have attempted in this study to develop protocols to decellularize large organs from pigs or humans and for the postproduction assessment of AC lung scaffolds. We used a prototype large organ bioreactor to fully decellularize full-sized pig or human trachea-lungs.

We then attempted to develop a standardized procedure for evaluation of pig or human trachea-lung scaffolds. A combination of bronchoscopy, PFT evaluation, MPM, and histology was used to examine key macroscopic and microscopic structural components we considered crucial for production of whole lung scaffolds. Using nonlinear optical microscopy methods of MPM and SHG we were able to evaluate the elastin and collagen microstructure of AC lung scaffolds. Elastin has a strong multiphoton AF and SHG provides specific contrast for fibrillar collagen in this tissue.[29] SHG has been extensively used to examine pathologic patterns of collagen fibers[24] and to identify fibrosis or other ECM abnormalities associated with lung disease.[30] The other advantages of MPM are that intact tissues can be imaged to depths >100 μm without physical sectioning, thereby allowing the natural 3D spatial relationship between these structural proteins to be maintained.[31] The combination of multiphoton AF with SHG provides a powerful way to noninvasively assess the interaction of these key lung structural proteins and to determine whether cell debris remained in the scaffolds. Additionally, imaging based on intrinsic signals eliminates the need for immunohistochemical labeling, which may not be desired if there is a need for longitudinal imaging of structural components.[32] MPM examinations of AC lung scaffold showed that we retained key ECM components involved in maintaining the strength and elasticity of the scaffold in each of the regions we examined. We also retained the ECM of both gross macroscopic

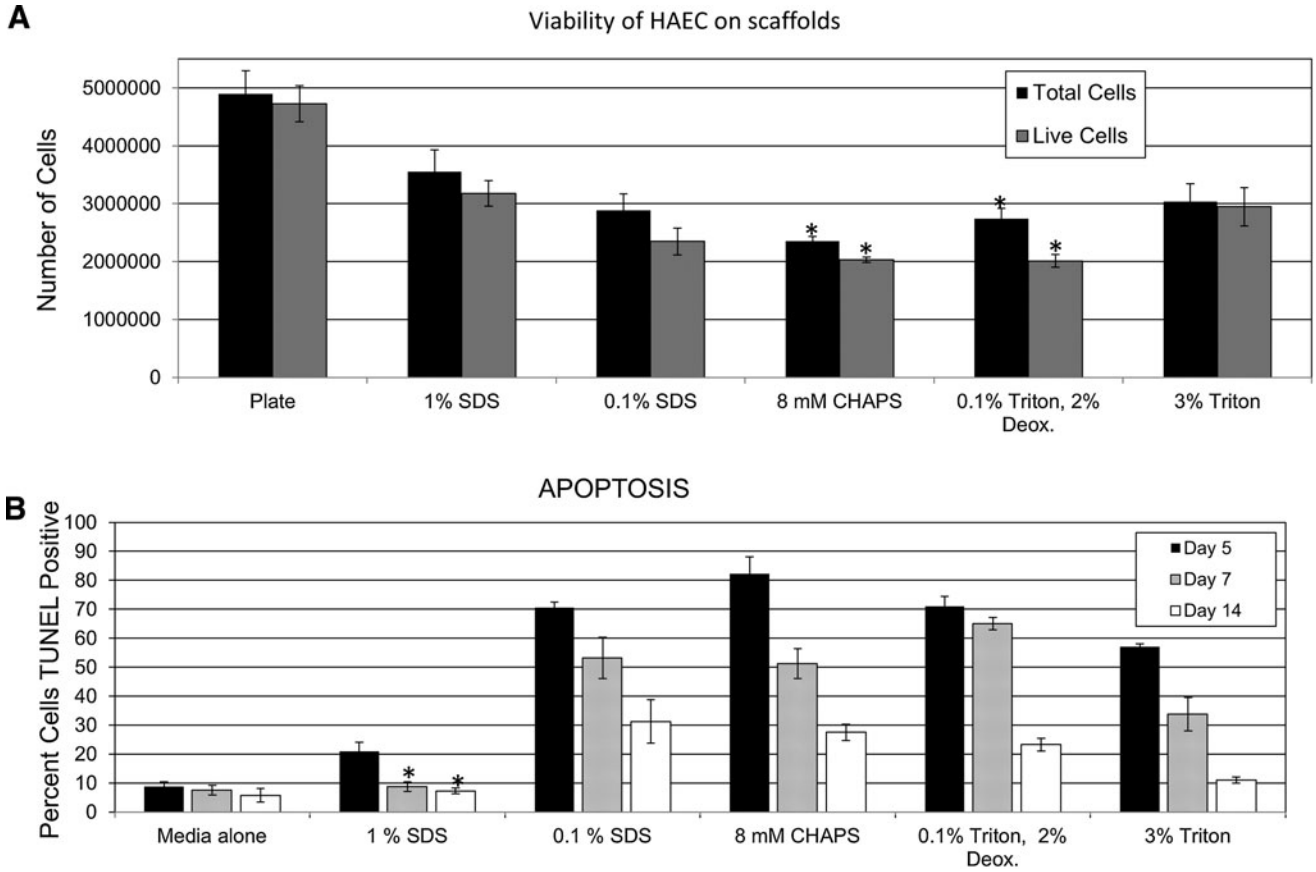

FIG. 11. Post production assessment of primary HAEC cultured on AC human scaffolds produced using different detergents. **(A)** Averaged data for evaluation of total number of cells and number of viable primary HAEC harvested at 7 days from scaffolds produced using different detergents. **(B)** Apoptosis was measured for cells isolated from HAEC/scaffold constructs produced on scaffolds generated using different detergents following 5, 7 or 14 days of decellularization treatment. Significantly less apoptosis was seen for AECs cultured on scaffolds produced using 1% SDS for 5 or 7 days ($*p < 0.05$) than for scaffolds produced using other detergents.

structures such as pleura, distal lung borders, trachea, and bronchi in addition to microscopic structures such as small blood vessels and bronchioles.

Postproduction assessment of human cellular and immune response to scaffolds is also an important consideration if biologically derived human lung scaffolds are to be used as therapeutic agents in the future. Natural scaffolds could induce unwanted cellular responses in patients due to production-related factors. The consequences of such immune reactions to a therapeutic material such as a biological scaffold may include lack of cell adhesion to scaffolds, poor viability, and induction of apoptosis or transient activation of immune cells, induction of proliferation, or production of factors that drive development of inflammation or cause graft rejection.

Scaffolds that have not been well decellularized or ones that have not been cleaned properly to remove residual detergent can exhibit low levels of cell adhesion or cell viability and high levels of apoptosis induction. Evaluation of cellular responses such as adhesion or viability to pig or human lung scaffold with cell types previously used to engineer lung tissue such as MESC indicated that both of these stem cells were able to attach and remain viable when grown on human lung scaffold produced using 1% SDS. Similar results were found for BMDMSC or primary type II HAEC. Interestingly, culture of these same cells on either Gelfoam or Matrigel was not as productive and fewer cells were found to attach to these scaffolds with significantly fewer cells viable at the end of the culture period. What was surprising was that cell attachment and viability for primary HAEC was better on the 3D AC lung matrices than plate culture. Attachment of primary type II HAECs on AC human scaffold produced using 1% SDS was not uniform at first but did result in survival of HAECs and eventual production of low levels of type I HAEC.

As part of our postproduction assessment we felt it was essential to develop a strategy for screening the human immune responses against biologically derived scaffolds. Evaluations for residual DNA or presence of cell debris are not satisfactory measures of the potential immunogenicity of AC lung. Scaffolds that contain detergent residue or cell debris may induce immunogenic responses and invoke immunological reactions that trigger inflammation and, potentially, graft rejection. We chose to examine the immune response of 10 MNL donors to the AC scaffold because careful immunogenicity evaluation should include data systematically collected from a sufficiently large number of donors. Data on efficacy and safety of reagents used in processing should be

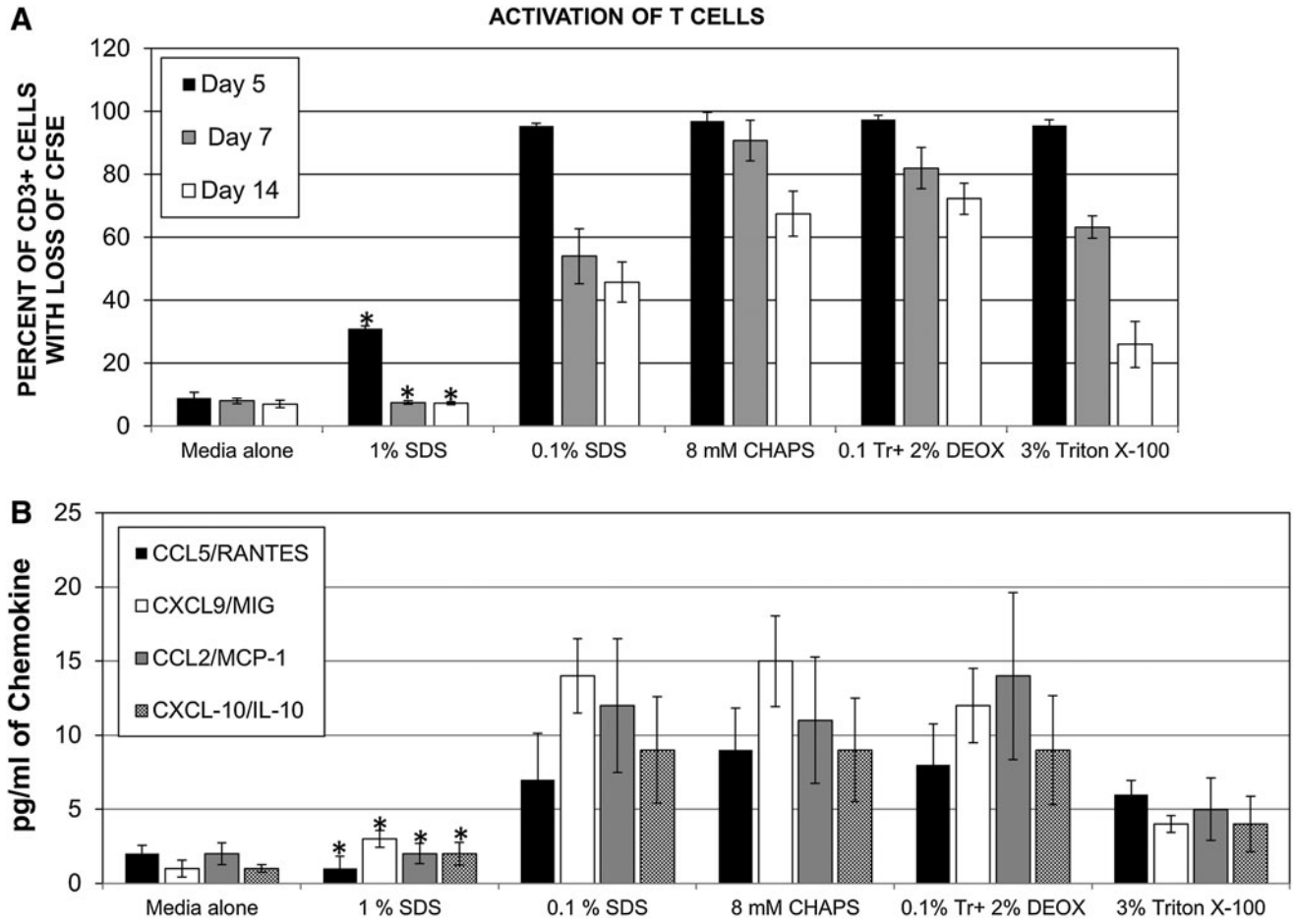

FIG. 12. Post production assessment of human immune cell activation. **(A)** Culture of human MNL with human AC distal lung produced using 1% SDS, 0.1% SDS, 8 mM CHAPS, and 0.1% Triton X-100 followed by 2% Deoxycholate or 3% Triton X-100 detergents to determine activation of CD3 T Cells. Values from cells isolated from triplicate cultures for each scaffold were averaged to determine loss of CFSE label. Human lung scaffold produced using 1% SDS induced significantly less activation of human MNLs than did scaffolds produced using other detergents. ($*p < 0.05$). **(B)** Examination of chemokine production by MNLs cultured with AC human lung scaffolds produced using different detergents. Lung scaffold produced using 1% SDS induced significantly lower levels of chemokines than did culture of MNLS with AC human lung scaffolds produced using other detergents ($*p < 0.05$). MNL, mononuclear leukocytes; CFSE, carboxyfluorescein succinimidyl ester.

collected for any decellularization protocol to fully understand the consequences of the immune response to reagents used. T cells are central to the process of transplant rejection through allorecognition of foreign antigens leading to their activation, and the orchestration of an effector response that results in graft damage.[33] Pathological hallmarks of transplant vasculopathy include development of marked inflammation in vessel walls.[34,35] The majority of infiltrating cells in these cases are CD3+ T cells, which become activated in response to a graft.[34,35] Chemokines play a critical role in recruitment of immune cells to injury or graft sites and CCL5, CXCL9, CCL2, and CXCL-10 have been shown to be important for T cell trafficking or T cell effector functions.[35] CXCL9 and CCL5 have even been found in alveolar lavages of allograft recipients with acute rejection.[35–37] It is for these reasons that we chose to examine the human immune response to AC lung scaffolds produced using a variety of detergents. We found that although 1% SDS caused significant loss of collagen in AC lung scaffolds it did not influence activation of T cells or production of chemokines important in T cell activation or graft rejection. The same was not true of other detergents and it is possible that the best decellularization protocol may be one that does not utilize detergents at all.

Summary and Conclusions

We have shown the feasibility of producing whole AC pig or human lung scaffolds for potential use in the engineering of lung tissue. The identification of a lung-appropriate scaffold such as the one we have produced is the first step to the ultimate goal of assembling a 3D vascularized functional living human organ construct applicable for future clinical implantation. There are some important issues that need to be examined relating to the current use of discarded lungs for research purposes and, potentially, in the future development of AC lung scaffolds for clinical use. Eventually, production standards, processing and sterilization methods, evaluation of product, and handling requirements prior to and after production of the AC scaffold will have to be

established. Policies will also need to be developed related to the process of tissue procurement for the purpose of producing AC scaffolds from discarded human lungs that do not meet the US standards for transplantation.

In the future we hope that discarded lungs not meeting the standards for transplantation will be used to generate AC scaffolds for the production of engineered lung tissue for both research and clinical applications.

Acknowledgments

This study was partially supported by grants from the National Institutes of Health (NIH U18TR000560-01), the Prepping to a biomedical PHD program (NIH, 1R25GM069285-04) and UTMB John Sealy Grant.

Disclosure Statement

No competing financial interests exist.

References

1. McCurry, K.R., Shearon, T.H., Edwards, L.B., Chan, K.M., Sweet, S.C., Valapour, M., Yusen, R., and Murray, S. Lung transplantation in the United States, 1998–2007. Am J Transplant **9,** 942, 2009.
2. Studer, S.M., Levy, R.D., McNeil, K., and Orens, J.B. Lung transplant outcomes: a review of survival, graft function, physiology, health-related quality of life and cost-effectiveness. Eur Respir J **24,** 674, 2004.
3. Zych, B., Popov, A.F., Stavri, G., Bashford, A., Bahrami, T., Amrani, M., De Robertis, F., Carby, M., Marczin, N., Simon, A.R., and Redmond, K.C. Early outcomes of bilateral sequential single lung transplantation after *ex-vivo* lung evaluation and reconditioning. J Heart Lung Transplant **31,** 274, 2012.
4. U.S. Organ and Transplantation Network and the Scientific Registry of Transplant Recipients. 2009. OPTN/SRTR annual report. Available at http://optn.transplant.hrsa.gov/ar2009/.
5. Medeiros, I.L., Pego-Fernandes, P.M., Mariani, A.W., Fernandes, F.G., do Vale Unterpertinger, F., Canzian, M., and Jatene, F.B. Histologic and functional evaluation of lungs reconditioned by *ex vivo* lung perfusion. J Heart Lung Transplant **31,** 305, 2012.
6. Steen, S., Ingemansson, R., Eriksson, L., Pierre, L., Algotsson, L., Wierup, P., Liao, Q., Eyjolfsson, A., Gustafsson, R., and Sjoberg, T. First human transplantation of a nonacceptable donor lung after reconditioning *ex vivo*. Ann Thorac Surg **83,** 2191, 2007.
7. Steen, S., Sjoberg, T., Pierre, L., Liao, Q., Eriksson, L., and Algotsson, L. Transplantation of lungs from a non-heart-beating donor. Lancet **357,** 825, 2001.
8. Cortiella, J., Niles, J., Cantu, A., Brettler, A., Pham, A., Vargas, G., Winston, S., Wang, J., Walls, S., and Nichols, J.E. Influence of acellular natural lung matrix on murine embryonic stem cell differentiation and tissue formation. Tissue Eng Part A **16,** 2565, 2010.
9. Zipfel, W.R., William, R.M., Christie, R., Nikitin, A.Y., Hyman, B.T., and Webb, W.W. Live tissue intrinsic emission microscopy using multiphoton-excited native fluorescence and second harmonic generation. PNAS **100,** 7075, 2003.
10. Sun, J., Shilagard, T., Bell, B., Motamedi, M., and Vargas, G. *In vivo* multimodal nonlinear optical imaging of mucosal tissue. Opt Express **12,** 2478, 2004.
11. Campagnola, P.J., and Loew, L.M. Second-harmonic imaging microscopy for visualizing biomolecular arrays in cells, tissues and organisms. Nat Biotech **21,** 1356, 2003.
12. Chen, X., Nadiarynkh, O., Plotnikov, S., and Campagnola, P.J. Second harmonic generation microscopy for quantitative analysis of collagen fibrillar structure. Nat Protoc **7,** 654, 2012.
13. Comhair, S.A., Xu, W., Mavrakis, L., Aldred, M.A., Asosingh, K., and Erzurum, S.C. Human primary lung endothelial cells in culture. Am J Respir Cell Mol Biol **46,** 723, 2012.
14. Nichols, J.E., Niles, J.A., and Roberts, N.J., Jr. Human lymphocyte apoptosis after exposure to influenza A virus. J Virol **75,** 5921, 2001.
15. Nichols, J.E., Fitzgerald, T.F., and Roberts, N.J., Jr. Human macrophage responses to vaccine strains of influenza virus: synthesis of viral proteins, interleukin-1 beta, interleukin-6, tumour necrosis factor-alpha and interleukin-1 inhibitor. Vaccine **11,** 36, 1993.
16. Nichols, J.E., Niles, J.A., and Cortiella, J. Engineering complex synthetic organs. In: Bernstein, H.S., ed. Tissue Engineering in Regenerative Medicine. New York: Humana Press, 2011, pp. 297–313.
17. Nichols, J.E., and Cortiella, J. Engineering of a complex organ: progress toward development of a tissue-engineered lung. Proc Am Thorac Soc. **5,** 723, 2008.
18. Cortiella, J.C., Nichols, J.E., Kojima, K., Bonassar, L.J., Dargon, P., Roy, A.K., Vacanti, M.P., Niles, J.A., and Vacanti, C.A. Tissue-engineered lung: an *in vivo* and *in vitro* comparison of polyglycolic acid and Pluronic F-127 hydrogel/somatic lung progenitor cell constructs to support tissue growth. Tissue Eng **12,** 1213, 2006.
19. Mondrinos, M.J., Kourzaki, S., Jiwanmall, E., Li, M., Dechadarevian, J.P., Lelkes, P.I., and Finck, C.M. Engineering three-dimensional pulmonary tissue constructs. Tissue Eng **12,** 717, 2006.
20. Kojima, K., Bonassar, L.J., Roy, A.K., Vacanti, C.A., and Cortiella, J. Autologous tissue-engineered trachea with sheep nasal chondrocytes. J Thorac Cardio Vasc Surg **123,** 117, 2002.
21. Macchiarini, P., Jungebluth, P., Go, T., Asnaghi, M.A., Rees, L.E., Cogan, T.A., Dodson, A., Martorell, J., Bellini, S., Parnigotto, P.P., Dickinson, S.C., Hollander, A.P., Mantero, S., Conconi, M.T., and Birchall, M.A. Clinical transplantation of a tissue-engineered airway. Lancet **372,** 2023, 2008.
22. Nichols, J.E., Niles, J.A., and Cortiella, J. Production and utilization of acellular lung scaffolds in tissue engineering. J Cell Biochem **113,** 2185, 2012.
23. Lwebuga-Mukasa, J.S., Ingbar, D.H., and Madri, J.A. Repopulation of a human alveolar matrix by adult rat type II pneumocytes *in vitro*: a novel system for type II pneumocyte culture. Exp Cell Res **162,** 423, 1986.
24. Price, A.P., England, K.A., Matson, A.M., Blazar, B.R., and Panoskaltsis-Mortari, A. Development of a decellularized lung bioreactor system for bioengineering the lung: the matrix reloaded. Tissue Eng Part A **16,** 2581, 2010.
25. Ott, H.C., Clippinger, B., Conrad, C., Schuetz, C., Pomerantseva, I., Ikonomou, L., Kotton, D., and Vacanti, J.P. Regeneration and orthotopic transplantation of a bioartificial lung. Nat Med **16,** 927, 2010.
26. Petersen, T.H., Calle, E.A., Zhao, L., Lee, E.J., Gui, L., Raredon, M.B., Gavrilov, K., Yi, T., Zhuang, Z.W., Breuer, C., Herzog, E., and Niklason, L.E. Tissue-engineered lungs for *in vivo* implantation. Science **329,** 538, 2010.

27. Song, J.J., Kim, S.S., Liu, Z., Madsen, J.C., Mathisen, D.J., Vacanti, J.P., and Ott, H.C. Enhanced *in vivo* function of bioartificial lungs in rats. Ann Thorac Surg **92,** 998, 2011.
28. Badylak, S.F., Taylor, D., and Uygun, K. Whole-organ tissue engineering: decellularization and recellularization of three-dimensional matrix scaffolds. Annu Rev Biomed Eng **13,** 27, 2011.
29. Konig, K., Schenke-Layland, K., Riemann, I., and Stock, U.A. Multiphoton autofluorescence imaging of intratissue elastic fibers. Biomaterials **26,** 495, 2005.
30. Strupler, M., Pena, A.M., Hernest, M., Tharaux, P.L., Martin, J.L., Beaurepaire, E., and Schanne-Klein, M.C. Second harmonic imaging and scoring of collagen in fibrotic tissues. Opt Express **15,** 4054, 2007.
31. Pena, A.M., Fabre, A., Debarre, D., Marchal-Somme, J., Crestani, B., Martin, J.L., Beaurepaire, E., and Schanne-Klein, M.C. Three-dimensional investigation and scoring of extracellular matrix remodeling during lung fibrosis using multiphoton microscopy. Microsc Res Tech **70,** 162, 2007.
32. Zoumi, A., Yeh, A., and Tromberg, B.J. Imaging cells and extracellular matrix *in vivo* by using second-harmonic generation and two-photon excited fluorescence. PNAS **99,** 11014, 2002.
33. Issa, F., Schiopu, A., and Wood, K.J. Role of T cells in graft rejection and transplantation tolerance. Expert Rev Clin Immunol **6,** 155, 2010.
34. Geleff, S., Draganovici, D., Jaksch, P., and Segerer, S. The role of chemokine receptors in acute lung allograft rejection. Eur Respir J **35,** 167, 2010.
35. Belperio, J.A., and Ardehali, A. Chemokines and transplant vasculopathy. Circ Res **103,** 454, 2008.
36. Luster, A. Chemokines-chemotactic cytokines that mediate inflammation. N Engl J Med **228,** 436, 1998.
37. Zlotnik, A., Morales, J., and Hendrick, J.A. Recent advances in chemokines and chemokine receptors. Crit Rev Immmunol **19,** 1, 1997.

Address correspondence to:
Joan E. Nichols, PhD
Department of Internal Medicine
University of Texas Medical Branch
Mail Route 0435
301 University Blvd.
Galveston, TX 66555-0435

E-mail: jnichols@utmb.edu

Received: April 19, 2012
Accepted: April 19, 2013
Online Publication Date: June 10, 2013